International Journal of Physical Sciences

Volume 9 Number 21 16 November, 2014

ISSN 1992-1950

Academic Journals

ABOUT IJPS

The **International Journal of Physical Sciences (IJPS)** is published weekly (one volume per year) by Academic Journals.

International Journal of Physical Sciences (IJPS) is an open access journal that publishes high-quality solicited and unsolicited articles, in English, in all Physics and chemistry including artificial intelligence, neural processing, nuclear and particle physics, geophysics, physics in medicine and biology, plasma physics, semiconductor science and technology, wireless and optical communications, materials science, energy and fuels, environmental science and technology, combinatorial chemistry, natural products, molecular therapeutics, geochemistry, cement and concrete research, metallurgy, crystallography and computer-aided materials design. All articles published in IJPS are peer-reviewed.

Contact Us

Editorial Office: ijps@academicjournals.org

Help Desk: helpdesk@academicjournals.org

Website: http://www.academicjournals.org/journal/IJPS

Submit manuscript online http://ms.academicjournals.me/

Editorial Board

International Journal of Physical Sciences

Table of Contents: Volume 9 Number 21, 16 November, 2014

ARTICLES

academicJournals

Vol. 9(21), pp. 459-465, 16 November, 2014
DOI: 10.5897/IJPS2014.4186
Article Number: F2A414948547
ISSN 1992 - 1950

http://www.academicjournals.org/IJPS

International Journal of Physical Sciences

Full Length Research Paper

Modifying the chaotic behavior in the quadrupole wiggler free-electron laser using ion-channel guiding

Mustafa Abu Safa

Department of Applied Physics, Palestine Polytechnic University, Hebron, P. O. Box198, Palestine.

Received 15 July, 2014; Accepted 5 November, 2014

The principles of free-electron laser (FEL) are explained. The motion of an individual electron in a FEL in a field configuration consisting of a quadrupole wiggler magnetic field is investigated. The general formulation of the dynamical problem is given. The Hamiltonian and Hamilton's equations of motion are derived. The problem of integrability and the Hamiltonian chaos is discussed. Upon plotting the Poincare' surface-of-section maps, the sensitivity for the initial conditions is shown. It has been confirmed that the presence of chaos is induced by the equilibrium self-electric and self-magnetic fields produced by the space charge and current of the electron beam. In this paper, the chaotic electron trajectories are modified by the effect of the ion-channel guiding. It is found that the effect of the ion-channel guiding is much better than the use of the axial guide magnetic field in which the motion is still chaotic when the self fields were taken into account.

Key words: Free-electron laser (FEL), wigglers, chaos, quadrupole.

INTRODUCTION

A free-electron laser (FEL) is a laser that shares the same optical properties as conventional lasers such as emitting a beam consisting of coherent electromagnetic radiation which can reach high power, but which uses some very different operating principles to form the beam. FELs use a relativistic electron beam as the lasing medium which move freely through a transverse periodic magnetic field, known as wiggler. The FEL has the widest frequency range of any laser type, and can be widely tunable. In recent years, a large number of researches on the FEL including both experimental and theoretical studies have been done. Experimental and theoretical works show numerous successful results at laboratories and research centers around the world (Marshall, 1985; Udholm et al., 1991; Bilikmen and Abu, 1992). FEL is remarkable for its special attributes, starting from its broad frequency tunability, high frequency, high power and wide bandwidth. These features are attractive for different medical, industrial and military applications. The FEL radiation is usually caused by passing the electron down a magnetic device known as an "undulator" or "wiggler", in which the electron is forced to execute a periodic oscillatory trajectory in space. The precise form for the wiggler field can take a variety of configurations, and FELs have been constructed both helically and linearly polarized wiggler fields. In principle, one can generate a periodic magnetic field by a helical winding of 2L wires (L = 1, 2,…). A magnetic field of this kind

*E-mail: mustafa@ppu.edu

exhibits a helical symmetry and depends on dimensionless coordinates ($k_w r$), and (φ- $k_w z$). The case L = 2 corresponds to a quadrupole which is used in this work. This kind of magnetic fields requires two pairs of helical windings with current flow in opposite directions in adjacent windings. A quadrupole magnetic field is widely used in conventional accelerators as well as in high current accelerators (Levush et al., 1985).

Theoretical investigations of FEL has been confined, principally, to the linear regime, however a full treatment is required to describe the interaction through the linear stages to saturation. Hamiltonian chaos has been an active area of research in physics and applied sciences. The classic work of Kol'mogorov, Arnold and Moser (KAM) shows that the generic phase space of non-integrable classical Hamiltonian systems, subject to small perturbations, contains three types of orbits: stable periodic orbits, stable quasi-periodic orbits (KAM tori), and chaotic orbits (Sagdeev et al., 1990). It is understood that chaotic behavior results from strong dependence on initial conditions. If any error develops in time, the nearby trajectories diverge exponentially and the orbit depends sensitively on the initial state. A very small randomness in the initial state is sufficient for this to occur. Hamiltonian with N degrees of freedom is integrable if it has N independent constants of motion in involution, e.g. the Poisson bracket of any two constants of them is 0. If the number of constants is less than N, the motion is non-integrable and part of the phase space is chaotic.

Earlier investigations of chaos in FEL have focused on chaotic behavior in particle orbits induced by sideband and radiation fields. The electromagnetic wave can also cause chaotic electron motion in the combined helical wiggler and axial guide field configuration (Takayama and Hiramatsu, 1988). This work examines the motion of relativistic test electron in a quadrupole wiggler FEL with and without axial guide magnetic field in addition to an ion-channel guiding. Of particular interest are the effects of the self-electric and self-magnetic fields produced by the space charge and current of the electron beam, where the Hamiltonian is found to be non-integrable and leading to chaotic motion. The replacement of the axial guiding field by the ion-channel guiding modified the chaotic behavior of the electron trajectories. The technique of the ion-channel guiding of an electron beam in FEL has become an area of great interest as it eliminates the need for conventional focusing magnets. Ion-channel guiding as an alternative to the conventional axial magnetic field guiding, was first proposed for FELs by Takayama and Hiramatsu (1988). This will make a capital and running cost less expensive because there is no power consumption (Takayama and Hiramatsu, 1988) (the strong axial magnetic fields of several kG). Motion of plasma electrons in such strong external fields may be characterized by magnetic trapping and an increase in relativistic mass due to rapid acceleration (Takayama and Hiramatsu, 1988). Jha and Kumar (1998) analyzed the effect of ion-channel guiding on a helically polarized wiggler magnetic field and obtained a substantial enhancement in peak growth rate as the ion-channel frequency approaches the wiggler frequency. Mohsenpour (2014) studied the steady-state orbits under the influence of the self fields in the presence of a one-dimensional helical wiggler with ion-channel guiding. The study shows that new unstable orbits are found. In this paper, the used wiggler is a quadrupole which is different and much complicated. The study shows that the replacement of the axial guiding field by the ion-channel guiding, modified the chaotic behavior of the electron trajectories.

Formulation of the problem

The vector potential solution of the static Maxwell equations in vacuum for a helical quadrupole field is in the form of (Sheng-Fuh et al., 1988):

$$\vec{A} = \vec{A}_w = A_r \hat{e}_r + A_\varphi \hat{e}_\varphi \tag{1}$$

$$A_r = -\frac{B_w}{k_w^2 r} I_2(2k_w r)\cos 2(\varphi - k_w z) \tag{2}$$

$$A_\varphi = \frac{B_w}{k_w} I_2'(2k_w r)\sin 2(\varphi - k_w z). \tag{3}$$

Where B_w is the wiggler amplitude, $k_w = 2\pi/\lambda_w$ is the wave number, I_2 is the modified Bessel function of second order, I'_2 is its derivative. Then the static magnetic fields are:

$$B_r = 2B_w I_2'(2k_w r)\cos 2(\varphi - k_w z), \tag{4}$$

$$B_\varphi = -\frac{2B_w}{k_w r} I_2'(2k_w r)\sin 2(\varphi - k_w z) \tag{5}$$

$$B_z = 2B_w I_2(2k_w r)\sin 2(\varphi - k_w z). \tag{6}$$

Self-fields

FEL operation often requires sufficiently large gain (growth rate), which increases when the beam current is increased. In high-current (high-density) regime, which is usually called Raman FEL, the electron motion can be altered significantly by the equilibrium self-field effects associated with beam space charge and current. One of the main purposes of this work is to examine the regular and irregular motion of an individual test electron in

combined field configuration and self-fields in the presence of ion-channel guiding.

It is readily shown from the steady state Maxwell equations that the E_s and the B_s can be expressed as (Saviz and Mehdian, 2005):

$$\vec{E}_s = -\frac{m_e\omega_{pb}^2}{2e}(x\hat{e}_x + y\hat{e}_y). \quad (7)$$

$$\vec{B}_s = \frac{m_e\omega_{pb}^2\beta_z}{2e}(y\hat{e}_x - x\hat{e}_y). \quad (8)$$

Where the suffix *s* is given for the self-fields, $\beta_z = V_z/c$ is the normalized beam velocity and $\omega_{pb} = (4\pi e^2 n_b/m_e)^{1/2}$ is the non-relativistic plasma frequency of the beam electrons.

The transverse electrostatic field generated by the ion-channel guiding E_i (the suffix i is given for the ion-channel) can be expressed by (Mehdian et al., 2001):

$$\vec{E}_i = 2\pi e n_i(x\hat{e}_x + y\hat{e}_y). \quad (9)$$

Here n_i is the charge density of the ion-channel guiding. In this formulation, the diamagnetic and paramagnetic effects are neglected.

The Hamiltonian representation

Frequently, equations of motion of a particle can be written quite simply in Hamiltonian form, in which the system of three second-order equations for the coordinates q_i, is represented by a system of six first-order equations for the three coordinate q_i and the three momenta p_i :

$$\frac{dp_i}{dt} = -\frac{\partial H}{\partial q_i}, \quad (10)$$

$$\frac{dq_i}{dt} = \frac{\partial H}{\partial p_i}, \quad (11)$$

Which are called the Hamilton's equation of motion, where the relativistic Hamiltonian is given by:

$$H = \left\{m^2c^4 + \left[c\vec{P} + e\vec{A}\right]^2\right\}^{1/2} - e\Phi \equiv \gamma mc^2 - e\Phi_s - e\Phi_i, \quad (12)$$

Where γ is the relativistic mass factor. The scalar potentials Φ_s , Φ_i and the vector potential A_s are:

$$\Phi_s(\vec{x}) = \frac{m_e\omega_{pb}^2}{4e}(x^2 + y^2) = \frac{m_e\omega_{pb}^2}{4e}r^2, \quad (13)$$

$$\Phi_i(\vec{x}) = -\frac{m_i\omega_{pi}^2}{4e}(x^2 + y^2) = -\frac{m_i\omega_{pb}^2}{4e}r^2, \quad (14)$$

$$\vec{A}_s(\vec{x}) = \beta_z\Phi_s(\vec{x})\hat{e}_z. \quad (15)$$

Now, the equations of motion for a test electron within the beam ($0 \le r < r_b$); (where r_b is the beam radius) can be derived for the Hamiltonian defined in Equation 12, with the vector potential $\vec{A} = \vec{A}_w + \vec{A}_s$, defined in Equations 1 and 15, and electrostatic potentials defined in Equations 13 and 14, respectively.

Because H is independent of time, the Hamiltonian is a constant of motion that is, H = constant, corresponds to the total energy (kinetic and potential energy) of the test electron.

For notational convenience in the subsequent analysis, we introduce the dimensionless Hamiltonian as follows:

$$\hat{H} = \left\{1 + \left[\frac{\vec{P}}{mc} + \hat{A}\right]^2\right\}^{1/2} - \hat{\Phi}_s - \hat{\Phi}_i. \quad (16)$$

The dimensionless variables and parameters defined by:

$$\hat{H} = \frac{H}{m_ec^2}, \quad \hat{A} = \frac{e\vec{A}}{m_ec^2}, \quad \hat{\Phi}_s = \frac{e\Phi_s}{m_ec^2} = \frac{\varepsilon_s k_w^2 r^2}{4}, \quad \hat{\Phi}_i = \frac{e\Phi_i}{m_ec^2} = -\frac{\xi_i k_w^2 r^2}{4}. \quad (17)$$

Where the dimensionless parameters $\xi_i = \frac{m_i\omega_{pi}^2}{m_ec^2k_w^2}$, and $\varepsilon_s = \frac{\omega_{pb}^2}{c^2k_w^2}$ characterize the strength of equilibrium self-fields and ion-channel guiding.

For $k_w r<1$, we can expand I_2 to second order in $k_w r$ and the normalized wiggler vector potential becomes:

$$\vec{A}_w \cong -\frac{a_\omega k_\omega r}{2}\cos 2(\varphi - k_\omega z)\hat{a}_r + \frac{a_\omega k_\omega r}{2}\sin 2(\varphi - k_\omega z)\hat{a}_\varphi. \quad (18)$$

Where $a_w = \frac{eB_w}{mc^2k_w}$ is the dimensionless measure for the

wiggler field amplitude.

In this sense, the Hamiltonian is written in the form:

$$\hat{H}(k_\omega r,\varphi,k_\omega z;\hat{P}_r,\hat{P}_\varphi,\hat{P}_z)=\left\{\left[\hat{P}_r-\frac{a_\omega k_\omega r}{2}\cos 2(\varphi-k_\omega z)\right]^2+\left[\frac{\hat{P}_\varphi}{k_\omega r}+\frac{a_\omega k_\omega r}{2}\sin 2(\varphi-k_\omega z)\right]^2+\left[\hat{P}_z+\frac{\beta_z\varepsilon_s k^2{}_\omega r^2}{4}\right]^2+1\right\}^{1/2}-\frac{\varepsilon_s k^2{}_\omega r^2}{4}+\frac{\xi_i k^2{}_\omega r^2}{4} \quad (19)$$

Where $\hat{P}_r=\frac{P_r}{mc}$, $\hat{P}_\varphi=\frac{P_\varphi}{mc}$, and $\hat{P}_z=\frac{P_z}{mc}$.

In order to find an additional constant of motion, it is useful to perform canonical transformations. Because the combination of (φ- k_wz) appears in Equation 19, we perform the canonical transformation to the new variables $(k_\omega r,\chi,k_\omega z';\hat{P}_r,\hat{P}_\chi,\hat{P}_{z'})$ defined by (Goldstein, 1980):

$$\begin{aligned} &k_\omega r=k_\omega r, && \chi=\varphi-k_\omega z, && k_\omega z'=k_\omega z,\\ &\hat{P}_r=\hat{P}_r, && \hat{P}_\chi=\hat{P}_\varphi, && \hat{P}_{z'}=\hat{P}_z+\hat{P}_\varphi \end{aligned} \quad (20)$$

Therefore, the Hamiltonian in the new variables can be expressed as:

$$\hat{H}(k_\omega r,\chi,k_\omega z';\hat{P}_r,\hat{P}_\chi,\hat{P}_{z'})=\left\{\left[\hat{P}_r-\frac{a_\omega k_\omega r}{2}\cos 2\chi\right]^2+\left[\frac{\hat{P}_\chi}{k_\omega r}+\frac{a_\omega k_\omega r}{2}\sin 2\chi\right]^2+\left[\hat{P}_{z'}-\hat{P}_\chi+\frac{\beta_z\varepsilon_s k^2{}_\omega r^2}{4}\right]^2+1\right\}^{1/2}-\frac{\varepsilon_s k^2{}_\omega r^2}{4}+\frac{\xi_i k^2{}_\omega r^2}{4} \quad (21)$$

Because $\hat{H}$ is independent of $k_\omega z'$, it follows that $\hat{P}_{z'}=const.$ Since no new canonical transformation is possible, then the third constant of motion is not available and the Hamiltonian is non-integrable, hence, chaotic orbits are possible.

Equations of motion

The Hamilton's equations of motion derived from the Hamiltonian in Equation 21, have the form:

$$\frac{d(k_\omega r)}{d\tau}=\frac{\partial\hat{H}}{\partial\hat{P}_r}=\frac{1}{\gamma}\left[\hat{P}_r-\frac{a_\omega k_\omega r}{2}\cos 2\chi\right], \quad (22)$$

$$\frac{d\chi}{d\tau}=\frac{\partial\hat{H}}{\partial\hat{P}_\chi}=\frac{1}{\gamma}\left\{\left[\frac{\hat{P}_\chi}{k_\omega r}+\frac{a_\omega k_\omega r}{2}\sin 2\chi\right]\left[\frac{1}{k_\omega r}\right]-\left[\hat{P}_z-\hat{P}_\chi+\frac{\beta_z\varepsilon_s k^2\omega r^2}{4}\right]^2\right\}, \quad (23)$$

$$\frac{d\hat{P}_r}{d\tau}=-\frac{\partial\hat{H}}{\partial(k_\omega r)}=\frac{\varepsilon_s k_\omega r}{2}-\frac{\xi_i k_\omega r}{2}-\frac{1}{\gamma}\left\{\left[\hat{P}_r-\frac{a_\omega k_\omega r}{2}\cos 2\chi\right]\left[-\frac{a_\omega}{2}\cos 2\chi\right]+\left[\frac{\hat{P}_\chi}{k_\omega r}+\frac{a_\omega k_\omega r}{2}\sin 2\chi\right]\left[-\frac{\hat{P}_\chi}{k^2\omega r^2}+\frac{a_\omega}{2}\sin 2\chi\right]+\left[\hat{P}_z-\hat{P}_\chi+\frac{\beta_z\varepsilon_s k^2\omega r^2}{4}\right]\left[\frac{\beta_z\varepsilon_s k_\omega r}{2}\right]\right\} \quad (24)$$

$$\frac{d\hat{P}_\chi}{d\tau}=\frac{\partial\hat{H}}{\partial\chi}=-\frac{1}{\gamma}\left\{\left[\hat{P}_r-\frac{a_\omega k_\omega r}{2}\cos 2\chi\right]\left[a_\omega k_\omega r\sin 2\chi\right]+\left[\frac{\hat{P}_\chi}{k_\omega r}+\frac{a_\omega k_\omega r}{2}\sin 2\chi\right]\left[a_\omega k_\omega r\cos 2\chi\right]\right\} \quad (25)$$

NUMERICAL SIMULATION

The set of equations of motion derived in the previous section are solved numerically in the following procedure.

First we consider an autonomous system defined by N simultaneous differential equations:

$$\begin{aligned} &\frac{dy_1}{dt}=f_1(y_1,...,y_n)\\ &\vdots\\ &\frac{dy_n}{dt}=f_n(y_1,...,y_n). \end{aligned} \quad (26)$$

A solution can be represented by a curve or a trajectory in an N-dimensional phase space. The successive intersections of the trajectory with the surface Σ defined by y_n-u=0, where u is a constant, are considered. It is not possible to specify in advance the variation of the dependent variable y_n over one integration step. This method is able to overcome the problem by dividing the (n-1) equations by the last one, resulting in a new set of equations in which t is considered as a dependent variable. The system of equations is integrated until a change in sign is detected for y_n-u=б, then one shifts to the new system for one step, taking Δ y_n =- б as an integration step. This is what is called Heno'n trick. This trick brings us exactly on the surface-of-section.

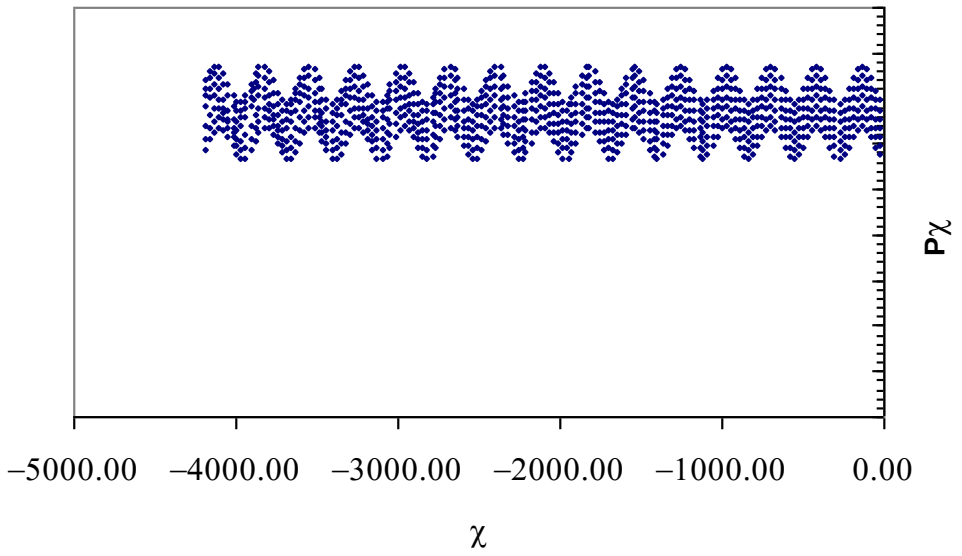

Figure 1. Poincare' surface-of –section plots in the $(\chi, \hat{P}_\chi)$ plane at $\hat{P}_r = 0$, for $\hat{H} = 3.0,\ a_w = 0.3,\ \beta_z = 0.94,\ \varepsilon_s = 0.0,$ and ξ =0.0.

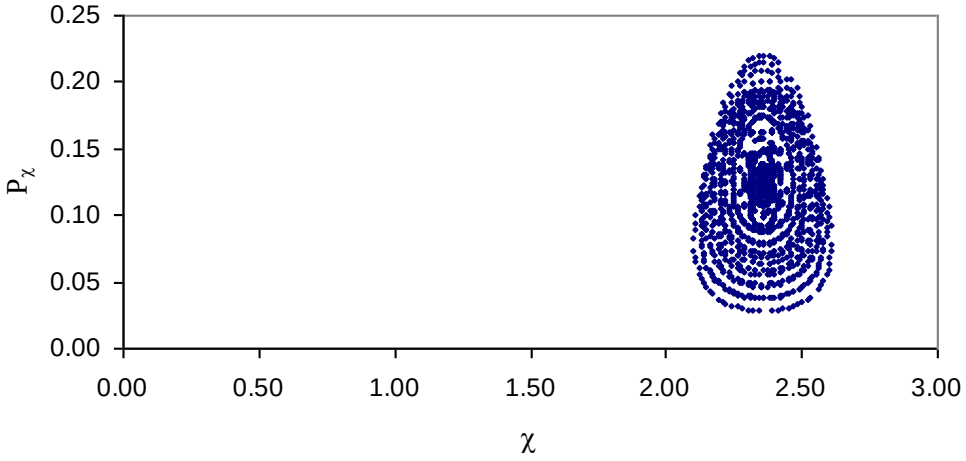

Figure 2. Poincare' surface-of –section plots in the $(\chi, \hat{P}_\chi)$ plane at $\hat{P}_r = 0$, for $\hat{H} = 3.0,\ a_w = 0.3,\ a_0 = 3.0,\ \beta_z = 0.94,\ \varepsilon_s = 0.0,$ and ξ =0.0.

RESULTS AND DISCUSSION

Poincare' surface-of -section maps have been generated by numerically integrating the equations of motion expressed in Equations 22 to 25. This analysis demonstrated the chaotic motion. The motion described by Equations 22 to 25 occurs in three-dimensional phase space $(\chi, \hat{P}_r, \hat{P}_\chi)$. Figure 1 shows the Poincare' surface-of-section plots in the $(\chi, \hat{P}_\chi)$ plane at $\hat{P}_r = 0$, for $\hat{H} = 3.0,\ a_w = 0.3$ with different initial conditions, while the effects of the self field and the ion-channel guiding are neglected. It is evident that these contours represent regular trajectories.

Figure 2 shows the Poincare' surface-of-section plots in the $(\chi, \hat{P}_\chi)$ plane at $\hat{P}_r = 0$, for $\hat{H} = 3.0,\ a_w = 0.3$, $a_0 = 0.3$ (the dimensionless measure for the axial guide field amplitude where the effect of the axial guide field is considered). The axial guide field is modifying the chaotic behavior for once the onset of chaos arising from large wiggler amplitudes, while it is found that the axial field

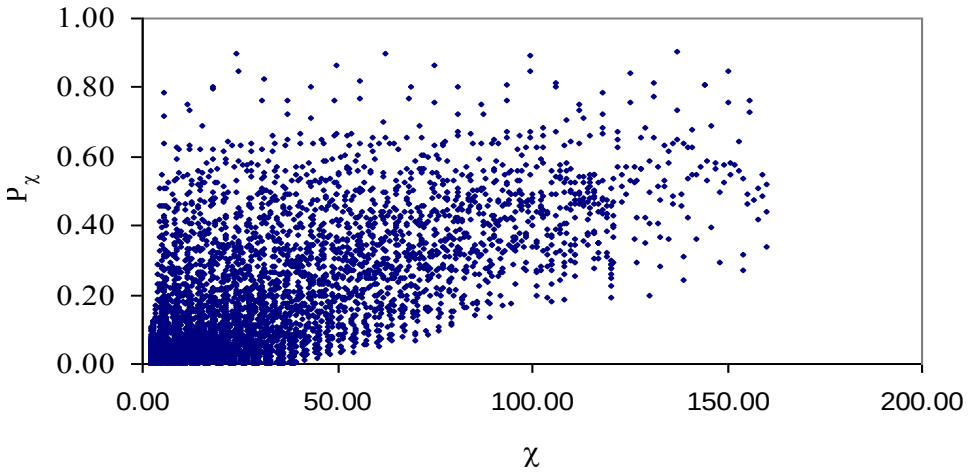

Figure 3. Poincare' surface-of –section plots in the $(\chi, \hat{P}_\chi)$ plane at $\hat{P}_r = 0$, for $\hat{H} = 3.0,\ a_w = 0.3,\ a_0 = 3.0,$, $\beta_z = 0.94,\ \varepsilon_s = 0.05,$ and ξ =0.0.

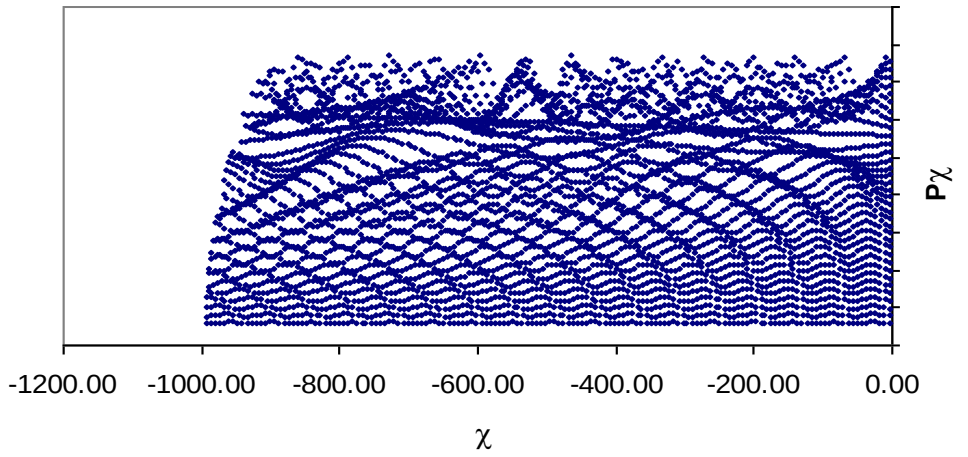

Figure 4. Poincare' surface-of -section plots in the $(\chi, \hat{P}_\chi)$ plane at $\hat{P}_r = 0$, for $\hat{H} = 3.0,\ a_w = 0.3,\ a_0 = 3.0,$, $\beta_z = 0.94,\ \varepsilon_s = 0.05,$ and ξ =0.07.

could not modify the chaotic behavior once the self-fields effects is considered.

Now, taking into account the effect of the self-fields, in the presence of the axial guide field, Figure 3 shows the chaotic behavior which could not be avoided. In Figure 4, the effect of the ion channel guiding which is used in place of the axial guiding field in the quadrupole wiggler configuration is considered and the orbits is shown to be closely to regular ones.

Conclusion

The use of the ion channel guiding is very useful in avoiding irregularity and chaotic behavior caused by self-fields. The axial guide field is working well just for the irregularity and chaos caused by strong wiggler amplitudes.

Conflict of Interest

The author has not declared any conflict of interest.

REFERENCES

Bilikmen S, Abu Safa M (1992). The nonlinear evolution of the free

electron laser amplifiers with both tapered planar wiggler and axial guide magnetic fields. Tr. J. Phys. (16):537.
Chen C, Schmidt G (1988). Chaotic electron motion in free electron lasers. Comments Plasma Phys. Controlled Fusion 12:83.
Goldstein H (1980). Classical Mechanics. Addison-Weslely.
Jha P, Kumar P (1998). Dispersion relation and growth in a free-electron laser with ion-channel guiding. Phys. Rev. E. 57(2):2256-2261. http://dx.doi.org/10.1103/PhysRevE.57.2256
Levush B, Antonsen TM, Manheimer WM, Sprangle P (1985). A free-electron laser with a rotating quadrupole wiggler. Phys. Fluids (28):2273. http://dx.doi.org/10.1063/1.865280
Marshall TC (1985). Free Electron Laser. New York, Macmillan. P. 23.
Mohsenpour T (2014). Steady-state electron trajectories in a free electron laser with ion-channel and axial magnetic field in a presence of self-fields. J. Theor. Appl. Phys. 8:128. http://dx.doi.org/10.1007/s40094-014-0128-6
Mehdian H, Esmelzadeh M, Willet JE (2001). Electron trajectories in a free-electron laser with planar wiggler and ion-channel guiding. Phys. Plasmas (8):3776. http://dx.doi.org/10.1063/1.1381424
Sagdeev RZ, Usikov DA, Zaslavsky GM (1990). Nonlinear Physics: From the Pendulum to Turbulence and Chaos. Harwood Academic Publishers. Second Printing, P. 125.
Saviz S, Mehdian H (2005). The effect of ion-channel guiding on chaotic electron trajectories in a free electron laser. Acta Physica Polonica A (107):895.
Sheng-Fuh C, Eldrige OC, Scharer JE (1988). Analysis and nonlinear simulation of a quadrupole wiggler FEL at millimeter wavelength. IEEE J. Quantum Electron. 24:2308. http://dx.doi.org/10.1109/3.8575
Takayama K, Hiramatsu S (1988). Ion-channel guiding in a steady-state free-electron laser. Phys. Rev. A. 37(1):173-177. http://dx.doi.org/10.1103/PhysRevA.37.173
Udholm P, Willett JE, Bilikmen S (1991). Free electron laser with longitudinal wiggler and finite axial magnetic field. J. Phys. D. (24):1278.

academicJournals

Vol. 9(21), pp. 466-474, 16 November, 2014
DOI: 10.5897/IJPS2014.4213
Article Number:417CC2548549
ISSN 1992 - 1950

http://www.academicjournals.org/IJPS

International Journal of Physical Sciences

Full Length Research Paper

Analytical investigation of convective heat transfer of a longitudinal fin with temperature-dependent thermal conductivity, heat transfer coefficient and heat generation

D. D. Ganji[1]* and A. S. Dogonchi[2]

[1]Department of Mechanical Engineering, Babol Noshirvani University of Technology, P. O. Box 484, Babol, Iran.
[2]Department of Mechanical Engineering, Mazandaran Institute of Technology, P. O. Box 747, Babol, Iran.

Received 15 September, 2014; Accepted 5 November, 2014

In this article, the heat transfer through a longitudinal fin is studied. The heat transfer coefficient, thermal conductivity and heat generation are variables and supposed to be temperature-dependent. The temperature distribution in fin with longitudinal rectangular profile was carried out by using the differential transformation method (DTM) which is an analytical solution technique. For validation of the analytical solution, the heat equation is solved numerically. The temperature distribution is shown for different values of the embedding parameters. The DTM results indicate that the fin tip temperature increases with an increase in the heat generation gradient. Results reveal that DTM is very effective and convenient. Comparison of the results (DTM and numerical) was shown that the analytical method and numerical data are in a good agreement with each other.

Key words: Fins, temperature dependent thermal properties, heat generation, analytical solutions, differential transformation method (DTM).

INTRODUCTION

Extended surfaces (also known as fins) are used to augment heat dissipation from a hot surface through its convective, radiative, or convective-radiative surface. In particular, fins are used extensively in various industrial applications such as the cooling of computer processors, air conditioning and oil carrying pipe lines. Several studies were performed on heat transfer using fins. Domairry and Fazeli (2009) solved the nonlinear straight fin differential equation to evaluate the temperature distribution and fin efficiency. Also, temperature distribution for annual fins with temperature-dependent thermal conductivity was studied by Ganji et al. (2011). The effects of temperature-dependent thermal conductivity of a moving fin and added radiative component to the surface heat loss have been studied by Aziz and Khani (2011). They applied the homotopy analysis method (HAM) to solve governing equations. Hatami et al. (2014) studied the temperature distribution

*Corresponding author. E-mail: ddg_davood@yahoo.com, Sattar.dogonchi@yahoo.com, Tel/Fax: +98 111 3234205.

for a fully wet, semi-spherical porous fin. Heat transfer and temperature distribution for circular convective-radiative porous fins was studied by Hatami and Ganji (2013). Hatami and Ganji (2014a) studied temperature distribution and refrigeration efficiency for fully wet circular porous fins with variable sections. Ghasemi et al. (2014) solved the nonlinear temperature distribution equation in a longitudinal fin with temperature-dependent internal heat generation and thermal conductivity using differential transformation method (DTM). Heat transfer and temperature distribution equations for longitudinal convective-radiative porous fins are solved by Hatami and Ganji (2014b). Heat transfer through porous fins with temperature-dependent heat generation was studied by Hatami et al. (2013). They employed DTM, collocation method (CM) and least square method (LS) for solving governing equations. Sharqawy and Zubair (2007) applied the analytical method for the annular fin with combined heat and mass transfer. Arslanturk (2005) and Rajabi (2007) obtained efficiency and fin temperature distribution by Adomian decomposition method (ADM) and the homotopy perturbation method (HPM) with temperature-dependent thermal conductivity. An analytical method for determining the optimum thermal design of convective longitudinal fin arrays is presented by Franco (2009). Lin and Lee (1999) investigated boiling on a straight fin with linearly varying thermal conductivity.

The concept of DTM was first introduced by Zhou (1986) and it was used to solve both linear and nonlinear initial value problems. This method can be applied directly to linear and nonlinear differential equation without requiring linearization, discretization, or perturbation and this is the main benefit of this method. Abbasov and Bahadir (2005) employed DTM to obtain approximate solutions of the linear and nonlinear equations related to engineering problems and they showed that the numerical results are in good agreement with the analytical solutions. Rashidi et al. (2010) solved the problem of mixed convection about an inclined flat plate embedded in a porous medium by DTM; they applied the Pade approximant to increase the convergence of the solution. Ghafoori et al. (2011) used the DTM for solving the nonlinear oscillation equation. Abdel-Halim (2008) has applied the DTM for different systems of differential equations and discussed the convergency of this method in several examples of linear and nonlinear systems of differential equations. Joneidi et al. (2009) used DTM for the analytical solution of convective straight fins with temperature-dependent thermal conductivity and comparing results with exact and numerical one. Their results reveal the capability, effectiveness, convenience and high accuracy of this method.

Moradi and Ahmadikia (2010) applied the DTM to solve the energy equation for a fin with three different profiles and temperature-dependent thermal conductivity. Balkaya et al. (2009) applied the DTM to analyze the vibration of an elastic beam supported on elastic soil. Borhanifar and Abazari (2011) employed DTM on some partial differential equations (PDEs) and their coupled versions.

The DTM is used to solve a wide range of physical problems. This method provides a direct scheme for solving linear and nonlinear deterministic and stochastic equations without linearization and yield convergent series solution rapidly.

The goal of this study is obtaining an analytical solution for temperature distribution of a fin with temperature-dependent thermal conductivity, heat transfer coefficient and heat generation. The effect of the range of values of heat transfer parameters on the temperature distribution is shown. Also, the DTM is applied to solve nonlinear problem analytically. To validate analytical results, the obtained DTM results are compared with numerical data.

PROBLEM DESCRIPTION

Consider a one-dimensional longitudinal fin, with an arbitrary profile $F(X)$ and cross-section area A_c as shown in Figure 1. The periphery of the fin is denoted by *P* and its length by *L*. The fin is attached to a fixed base surface of temperature T_b and extend to an ambient fluid of temperature T_a. The fin thickness is given by δ and the base thickness is δ_b. The $1\text{-}D$ steady state energy equation for the fin with internal heat generation can be expressed as:

$$\frac{\partial}{\partial X}\left(\frac{\delta_b}{2}F(X)K(T)\frac{\delta T}{\delta X}\right)-\frac{P}{A_c}H(T)\left(T-T_a\right)+q^*=0,\quad 0\le X\le L. \tag{1}$$

Where K, H and q^* are the non-uniform thermal conductivity, heat transfer coefficients and heat generation depending on the temperature, *T* is the temperature distribution and X is the spatial variable. An insulated fin at one end with the base temperature at the other implies boundary condition which is given by (Kraus, 2001):

$$T(L)=T_b \qquad , \ \frac{\partial T}{\partial X}\Big|_{X=0}=0. \tag{2}$$

Because of the heat generation varying with temperature, so we have:

$$q^*=q_a^*\left(1+\varepsilon\left(T-T_a\right)\right) \tag{3}$$

For simplifying the above equations, some dimensionless parameters are introduced as follows:

$$x=\frac{X}{L},\ \theta=\frac{T-T_a}{T_b-T_a},\ h=\frac{H}{h_b},\ k=\frac{K}{k_a},\ M^2=\frac{Ph_bL^2}{A_ck_a},\ R=\frac{q_a^*A_c}{h_bP(T_b-T_a)}, \tag{4}$$

$$\varepsilon_R=\varepsilon(T_b-T_a),\ f(x)=\frac{\delta_b}{2}F(X)$$

Equation 1 reduces to:

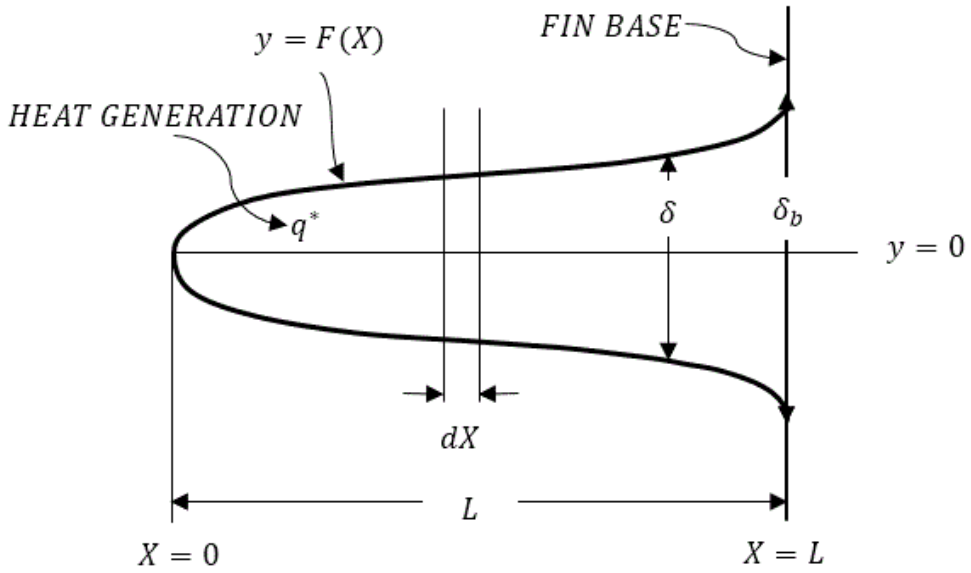

Figure 1. Schematic representation of a longitudinal fin with arbitrary profile *F(X)*.

$$\frac{\partial}{\partial x}\left(f(x)k(\theta)\frac{\delta\theta}{\delta x}\right)-M^2h(\theta)\theta+M^2R\left(1+\varepsilon_R\theta\right)=0,\quad 0\le x\le 1. \tag{5}$$

And the boundary conditions become

$$\theta(1)=1 \qquad , \frac{\partial\theta}{\partial x}\Big|_{x=0}=0. \tag{6}$$

Where *M* is the thermogeometric fin parameter, θ is the dimensionless temperature, *X* is the dimensionless spatial variable, q_a^* is the internal heat generation at temperature T_a, *k* is the dimensionless thermal conductivity, k_a is the thermal conductivity of the fin at ambient temperature, h_b is the heat transfer coefficient at the fin base. For most industrial application, the heat transfer coefficient maybe given as a power law (Unal, 1987):

$$H(T)=h_b\left(\frac{T-T_a}{T_b-T_a}\right)^n \tag{7}$$

Where *n* and h_b are constants. The constant n may vary between -6.6 and 5. However, in most practical applications it lies between -3 and 3 (Unal, 1987). The exponent n represents laminar film boiling or condensation when $n=-1/4$, laminar natural convection when $n=1/4$, turbulent natural convection when $n=1/3$, nucleate boiling when $n=2$, radiation when *n* = 3 and *n* = 0 implies a constant heat transfer coefficient. Exact solutions may be constructed for the steady-state one-dimensional differential equation describing temperature distribution in a straight fin when the thermal conductivity is a constant and the exponent of the heat transfer coefficient is given by $n=-1,0,1$ or 2 (Unal, 1987).

In dimensionless variables we have $h(\theta)=\theta^n$. Also, for many engineering applications, the thermal conductivity may depend linearly on temperature, that is;

$$K(T)=k_a\left[1+\gamma(T-T_a)\right] \tag{8}$$

The dimensionless thermal conductivity given by the linear function of temperature is $k(\theta)=1+\beta\theta$, where the thermal conductivity gradient is $\beta=\gamma(T_b-T_a)$.

As such, the governing equation is given by:

$$\frac{\partial}{\partial x}\left(f(x)(1+\beta\theta)\frac{\delta\theta}{\delta x}\right)-M^2\theta^{n+1}+M^2R\left(1+\varepsilon_R\theta\right)=0,\ 0\le x\le 1 \tag{9}$$

FUNDAMENTAL OF DIFFERENTIAL TRANSFORMATION METHOD (DTM)

Let $x(t)$ be analytic in a domain *D* and let $t=t_i$ represent any point in *D*. The function $x(t)$ is then represented by one power series whose center is located at t_i. The Taylor series expansion function of $x(t)$ is in form of:

$$x(t)=\sum_{k=0}^{\infty}\frac{(t-t_i)^k}{k!}\left[\frac{d^kx(t)}{dt^k}\right]_{t=t_i} \qquad \forall t\in D \tag{10}$$

The particular case of Equation 10 when $t_i=0$ is referred to as the Maclaurin series of $x(t)$ and is expressed as:

Table 1. The fundamental operations of the differential transform method.

Original function	Transformed function
$w(t)=\alpha u(t)\pm\beta v(t)$	$W(k)=\alpha U(k)\pm\beta V(k)$
$w(t)=\frac{d^m u(t)}{dt^m}$	$W(k)=\frac{(k+m)!}{k!}U(k+m)$
$w(t)=u(t)v(t)$	$W(k)=\sum_{l=0}^{k}U(l)V(k-l)$
$w(t)=t^m$	$W(k)=\delta(k-m)=\begin{cases}1, & \text{if } k=m\\ 0, & \text{if } k\neq m\end{cases}$
$w(t)=\exp(t)$	$W(k)=\frac{1}{k!}$

$$x(t)=\sum_{k=0}^{\infty}\frac{t^k}{k!}\left[\frac{d^k x(t)}{dt^k}\right]_{t=0} \qquad \forall t\in D \tag{11}$$

As explained in Zhou (1986) and Abdel-Halim (2004), the differential transformation of the function $x(t)$ is defined as follows:

$$X(k)=\sum_{k=0}^{\infty}\frac{H^k}{k!}\left[\frac{d^k x(t)}{dt^k}\right]_{t=0} \tag{12}$$

Where $x(t)$ is the original function and $X(k)$ is the transformed function. The differential spectrum of $X(k)$ is confined within the interval $t\in[0,H]$, where *H* is a constant. The differential inverse transform of $X(k)$ is defined as follows:

$$x(t)=\sum_{k=0}^{\infty}\left(\frac{t}{H}\right)^k X(k) \tag{13}$$

It is clear that the concept of the differential transformation is based upon the Taylor series expansion. The values of function $X(k)$ at values of argument *k* are referred to as discrete, that is, $X(0)$ is known as the zero discrete, $X(1)$ as the first discrete, etc. the more discrete available, the more precise it is possible to restore the unknown function. The function $x(t)$ consists of *T*-function $X(k)$, and its value is given by the sum of the *T*-function with $(t/H)^k$ as its coefficient. In real applications, at the right choice of constant *H*, the larger values of argument k the discrete of spectrum reduce rapidly. The function $x(t)$ is expressed by a finite series and Equation 13 can be written as:

$$x(t)=\sum_{k=0}^{n}\left(\frac{t}{H}\right)^k X(k) \tag{14}$$

Mathematical operations performed by differential transform method are listed in Table 1.

ANALYTICAL SOLUTION

By 1-D transform of Equation 9 considered by using the related definition in Table 1, we have the following:

(1) Rectangular profile ($f(x)=1$), case $n=1$

$$(K+1)(K+2)\Theta(K+2)+\beta\left(\sum_{i=0}^{K}\Theta(i)(K+1-i)(K+2-i)\Theta(K+2-i)\right)+\beta\left(\sum_{i=0}^{K}(i+1)\Theta(i+1)(K+1-i)\Theta(K+1-i)\right)$$
$$-M^2\left(\sum_{i=0}^{K}\Theta(i)\Theta(K-i)\right)+M^2R\left(\delta(K)+\varepsilon_R\Theta(K)\right)=0, \tag{15}$$

(2) Rectangular profile ($f(x)=1$), case $n=2$

$$(K+1)(K+2)\Theta(K+2)+\beta\left(\sum_{i=0}^{K}\Theta(i)(K+1-i)(K+2-i)\Theta(K+2-i)\right)+\beta\left(\sum_{i=0}^{K}(i+1)\Theta(i+1)(K+1-i)\Theta(K+1-i)\right)$$
$$-M^2\left(\sum_{j=0}^{K}\Theta(K-j)\sum_{i=0}^{j}\Theta(i)\Theta(j-i)\right)+M^2R\left(\delta(K)+\varepsilon_R\Theta(K)\right)=0, \tag{16}$$

In the above equations $\Theta(K)$ is transformed function of $\Theta(x)$. The transformed boundary condition takes the form:

$$\Theta(1)=0 \tag{17}$$

$$\sum_{i=0}^{\infty}\Theta(i)=1 \tag{18}$$

Supposing that $\Theta(0)=a$ and using Equations 17 and 18, another value of $\Theta(i)$ can be calculated.

The value of a can be calculated using Equation 18. Thus, we end up having the following:

(1) Rectangular profile, case $n=1$

$$\Theta(2)=-\frac{1}{2}\frac{M^2\left(-a^2+R+R\varepsilon_R a\right)}{1+\beta a}$$
$$\Theta(3)=0$$
$$\Theta(4)=-\frac{1}{24}\frac{M^4\left(-a^2+R+R\varepsilon_R a\right)\left(2a-\beta a^2+3\beta R+2\beta R\varepsilon_R a-R\varepsilon_R\right)}{\left(1+\beta a\right)^3} \tag{19}$$

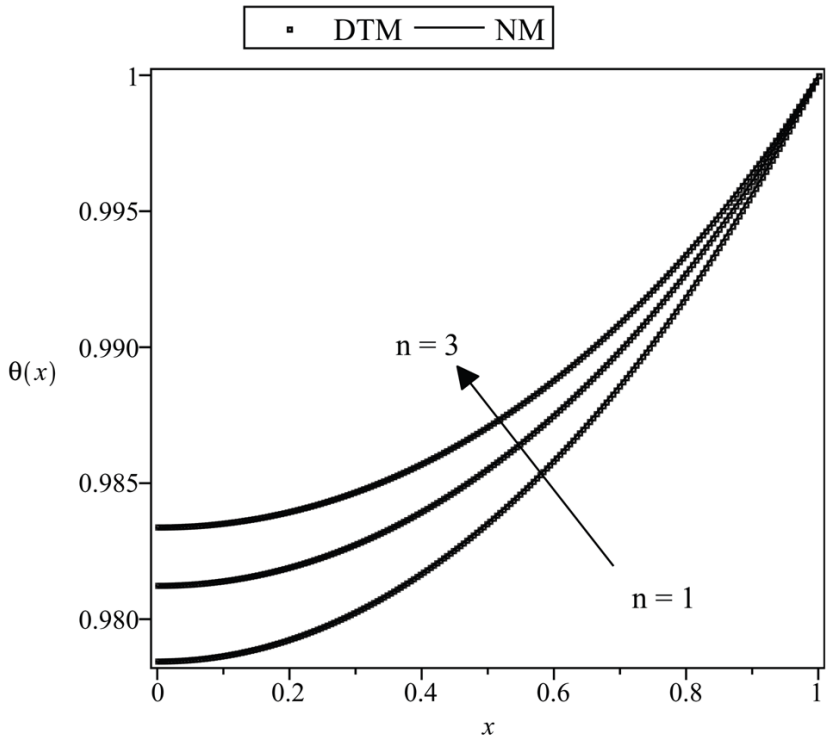

Figure 2. Comparison of (x) obtained by the DTM with numerical solution in a longitudinal rectangular fin when M = 1, β = 1, R = 0.8, ε_R = 0.1.

(2) Rectangular profile, case $n=2$

$$\Theta(2)=-\frac{1}{2}\frac{M^2\left(-a^3+R+R\varepsilon_R a\right)}{1+\beta a}$$
$$\Theta(3)=0$$
$$\Theta(4)=-\frac{1}{24}\frac{M^4\left(-a^3+R+R\varepsilon_R a\right)\left(3a^2+3\beta R+2\beta R\varepsilon_R a-R\varepsilon_R\right)}{\left(1+\beta a\right)^3} \quad (20)$$

From the above continuing process, substituting Equation 19 in Equation 14 for *H* = 1, we can obtain the closed form of the solution:

(1) Rectangular profile, case $n=1$

$$\theta(x)=a-\frac{1}{2}\frac{x^2M^2\left(-a^2+R+R\varepsilon_R a\right)}{1+\beta a} \quad (21)$$
$$-\frac{1}{24}\frac{x^4M^2\left(-a^2+R+R\varepsilon_R a\right)\left(2a-\beta a^2+3\beta R+2\beta R\varepsilon_R a-R\varepsilon_R\right)}{\left(1+\beta a\right)^3}+\ldots$$

In order to obtain the value a, we used Equation 18. Then, we will have:

$$\theta(1)=a-\frac{1}{2}\frac{M^2\left(-a^2+R+R\varepsilon_R a\right)}{1+\beta a} \quad (22)$$
$$-\frac{1}{24}\frac{M^2\left(-a^2+R+R\varepsilon_R a\right)\left(2a-\beta a^2+3\beta R+2\beta R\varepsilon_R a-R\varepsilon_R\right)}{\left(1+\beta a\right)^3}+\ldots=1$$

Solving Equation 22 by Maple software gives the value of a. For other cases the same process is used to obtain the value of a and temperature distribution.

RESULTS AND DISCUSSION

In this paper, the steady-state heat transfer in a longitudinal rectangular fin was studied. The dependence of the thermal conductivity, heat transfer coefficients and heat generation on the temperature rendered the problem highly nonlinear. The effects of the thermogeometric fin parameter (M), thermal conductivity gradient (β), heat generation gradient (ε_R) and *R* are investigated on the temperature distribution. To validate the analytical results, the temperature distribution through the longitudinal rectangular fin is compared with the numerical solution. The results are well matched with the results carried out by numerical solution as shown in Figure 2 and Table 2. In this table, error is introduced as follows:

$$\%Error=\left|\frac{\theta(x)_{NM}-\theta(x)_{DTM}}{\theta(x)_{NM}}\right|\times 100.$$

This accuracy gives high confidence in the validity of this

Table 2. Comparison between DTM and numerical results of θ(x) for rectangular profile when M=1, β=1, R=0.8 and $\varepsilon_R = 0.1$

$f(x)=1$		$n=1$			$n=2$			$n=3$	
x	**NM**	**DTM**	**Error (%)**	**NM**	**DTM**	**Error (%)**	**NM**	**DTM**	**Error (%)**
0	0.9784318	0.9784798	0.0048984	0.9812073	0.9812627	0.0056476	0.9833487	0.9834069	0.005912
0.1	0.9786395	0.9786799	0.0041301	0.9813846	0.9814303	0.0046542	0.9835028	0.9835497	0.0047697
0.2	0.9792382	0.9792822	0.0044861	0.9818847	0.9819353	0.0051584	0.983928	0.983981	0.0053895
0.3	0.9802475	0.9802919	0.0045252	0.982733	0.9827848	0.005271	0.9846536	0.9847085	0.0055756
0.4	0.9816774	0.981718	0.0041318	0.9839427	0.9839903	0.004838	0.985695	0.9857458	0.0051467
0.5	0.9835368	0.9835732	0.0036963	0.9855253	0.9855683	0.0043627	0.9870656	0.9871118	0.0046793
0.6	0.9858406	0.9858738	0.0033713	0.9875004	0.9875404	0.0040514	0.988788	0.9888318	0.0044207
0.7	0.9886144	0.9886403	0.0026174	0.9899023	0.9899337	0.0031732	0.9909028	0.9909375	0.0034959
0.8	0.9918745	0.991897	0.0022701	0.9927527	0.9927809	0.0028364	0.9934361	0.993468	0.003207
0.9	0.9956481	0.9956725	0.0024481	0.9960891	0.9961211	0.0032124	0.9964326	0.9964702	0.0037711
1	1	1	0	1	1	0	1	1	0

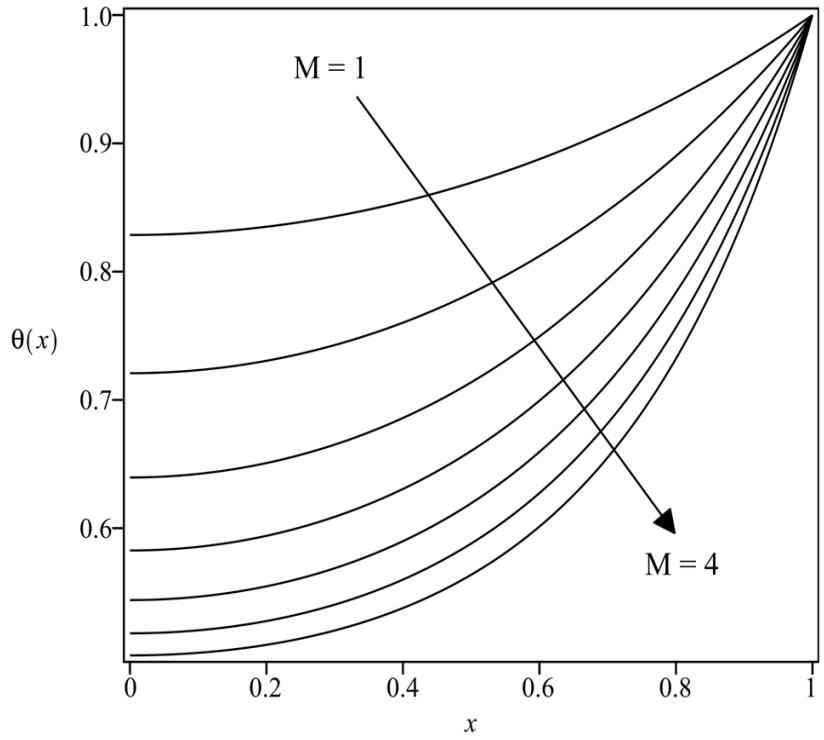

Figure 3. Temperature distribution in a longitudinal rectangular fin for varying values of thermo-geometric parameter (M) when n = 1, β = 0.5, R = 0.2, ε_R = 0.2.

problem, and reveals an excellent agreement in engineering accuracy.

The effect of thermo-geometric parameter (M) on temperature distribution is shown in Figure 3. It is illustrated that the magnitude of temperature is increased with decreasing the thermo-geometric parameter (M). Note that the thermo-geometric fin parameter $M = (Bi)^{1/2} E$, where $Bi = h_b \delta / k_a$ is the Biot number and $E = L/\delta$ is the aspect ratio or the extension factor. Undoubtedly, small values of M correspond to the relatively short and thick fins of high conductivity and high values of M correspond to longer and thin fins of poor conductivity (Mills, 1995). A fin is an excellent squanderer at small values of M. As M increases the convective heat loss increases and the temperature profile becomes steeper reflecting high base heat flow rates. In Figure 4,

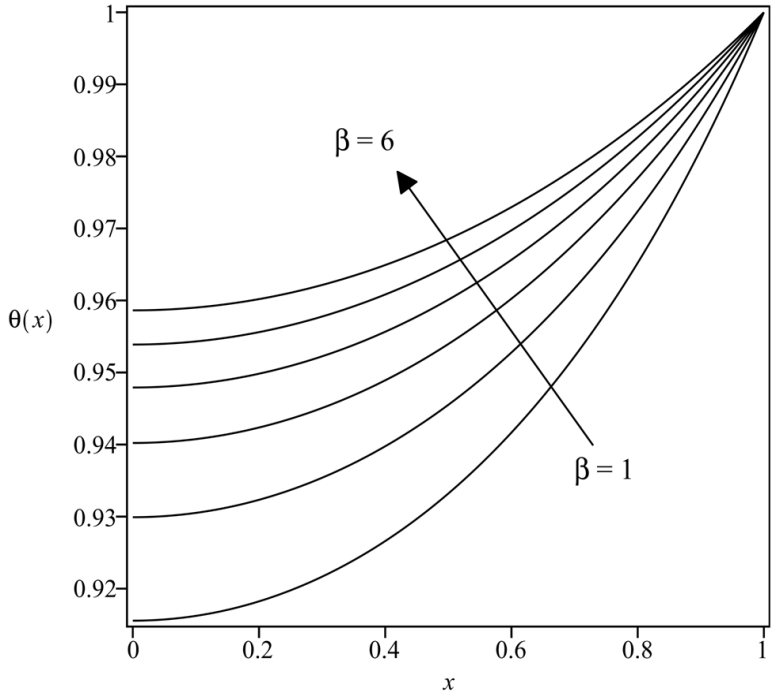

Figure 4. Temperature distribution in a longitudinal rectangular fin for varying values of β when n = 1, M = 2, R = 0.5, ε_R = 0.6.

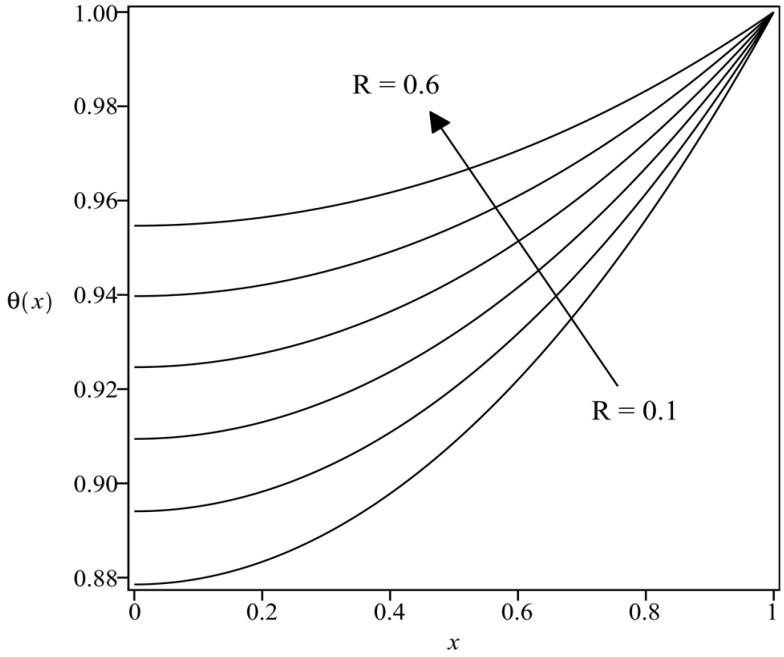

Figure 5. Temperature distribution in a longitudinal rectangular fin for varying values of R when n = 1, M = 1, β = 2, ε_R = 0.1.

we observe that the temperature in the fin increases with the increasing values of the thermal conductivity gradient (β). Figure 5 illustrates the variation of the temperature distribution with R. In addition, the effect of the heat generation gradient on the temperature distribution is shown in Figure 6. With a decrease in the ε_R, the losing

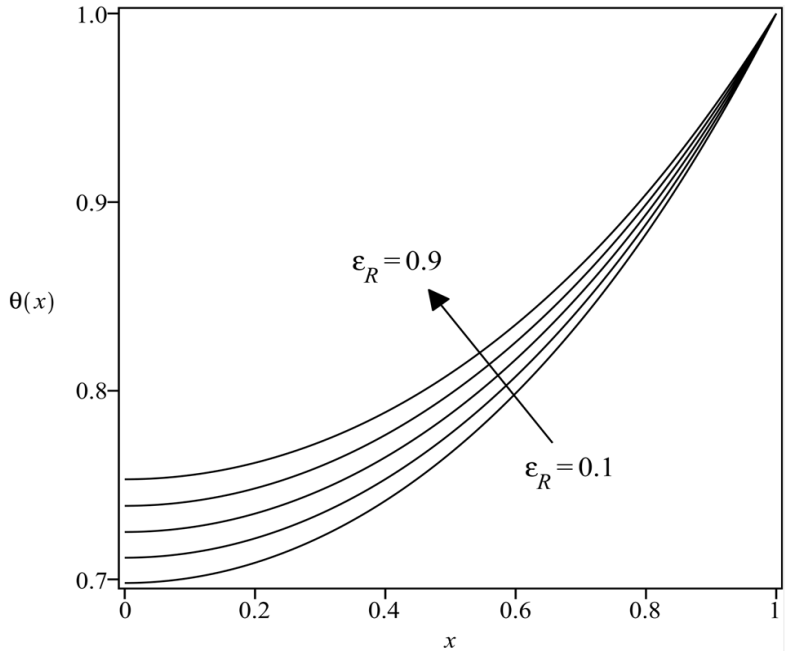

Figure 6. Temperature distribution in a longitudinal rectangular fin for varying values of ε_R when n = 1, M = 2, β = 1.5, R = 0.2.

heat from fin surface becomes stronger, thus the fin temperature decreases.

Conclusion

In this study, the DTM was applied to solve the heat transfer problem in a rectangular fin with temperature-dependent thermal conductivity, heat transfer coefficient and heat generation. Also, this problem is solved by a numerical method and some conclusions were summarized as follows:

(a) The DTM is a powerful approach for solving nonlinear differential equation, such as this problem. Also, it can be observed that there is good agreement between the present and numerical results.
(b) Increasing thermo-geometric parameter leads to a decrease in temperature distribution.
(c) By increasing thermal conductivity and heat generation gradient, temperature distribution increase.

Conflict of Interest

The author(s) have not declared any conflict of interest.

REFERENCES

Abbasov A, Bahadir AR (2005). The investigation of the transient regimes in the nonlinear systems by the generalized classical method. Math. Probl. Eng. 5:503-519. http://dx.doi.org/10.1155/MPE.2005.503

Abdel-Halim HIH (2004). Differential transformation technique for solving higher-order initial value problems, Appl. Math. Comput. 154(2):299-311. http://dx.doi.org/10.1016/S0096-3003(03)00708-2

Abdel-Halim HIH (2008). Application to differential transformation method for solving systems of differential equations. Appl. Math. Model. 32(12):2552-2559. http://dx.doi.org/10.1016/j.apm.2007.09.025

Arslanturk C (2005). A decomposition method for fin efficiency of convective straight fins with temperature-dependent thermal conductivity. Int. Commun. Heat Mass Transfer. 32(6):831-841. http://dx.doi.org/10.1016/j.icheatmasstransfer.2004.10.006

Aziz A, Khani F (2011). Convection-radiation from a continuously moving fin of a variable thermal conductivity. J. Franklin Inst. 348(4):640-651. http://dx.doi.org/10.1016/j.jfranklin.2011.01.008

Balkaya M, Kaya MO, Saglamer A (2009). Analysis of the vibration of an elastic beam supported on elastic soil using the differential transform method. Arch. Appl. Mech. 79:135-146. http://dx.doi.org/10.1007/s00419-008-0214-9

Borhanifar A, Abazari R (2011). Exact solutions for non-linear Schrdinger equations by differential transformation method. J. Appl. Math. Comput. 35:37-51. http://dx.doi.org/10.1007/s12190-009-0338-2

Domairry G, Fazeli M, (2009). Homotopy analysis method to determine the fin efficiency of convective straight fins with temperature-dependent thermal conductivity. Comm. Nonlinear Sci. Numer. Simulat. 14(2):489-499. http://dx.doi.org/10.1016/j.cnsns.2007.09.007

Franco A (2009). An analytical method for the optimum thermal design of convective longitudinal fin arrays. Heat Mass Transfer 45(12):1503-1517. http://dx.doi.org/10.1007/s00231-009-0526-5

Ganji DD, Ganji ZZ, Ganji HD (2011). Determination of temperature distribution for annual fins with temperature-dependent thermal conductivity by HPM. Therm. Sci. 15(1):111-115.

Ghafoori S, Motevalli M, Nejad MG, Shakeri F, Ganji DD, Jalaal M (2011). Efficiency of differential transformation method for nonlinear oscillation: comparison with HPM and VIM. Curr. Appl. Phys. 1:965-971. http://dx.doi.org/10.1016/j.cap.2010.12.018

Ghasemi SE, Hatami M, Ganji DD (2014). Thermal analysis of

convective fin with temperature-dependent thermal conductivity and heat generation. Case Studies in Therm. Eng. 4:1-8. http://dx.doi.org/10.1016/j.csite.2014.05.002
Hatami M, Ganji DD (2013). Thermal performance of circular convective-radiative porous fins with different section shapes and materials. Energy Convers. Manage. 76:185-193. http://dx.doi.org/10.1016/j.enconman.2013.07.040
Hatami M, Ganji DD (2014a). Investigation of refrigeration efficiency for fully wet circular porous fins with variable sections by combined heat and mass transfer analysis. int. J. Refrig. 40:140-151. http://dx.doi.org/10.1016/j.ijrefrig.2013.11.002
Hatami M, Ganji DD (2014b). Thermal behavior of longitudinal convective-radiative porous fins with different section shapes and ceramic materials (SiC and Si3N4). Ceram. Int. 40(5):6765-6775. http://dx.doi.org/10.1016/j.ceramint.2013.11.140.
Hatami M, Hasanpour A, Ganji DD (2013). Heat transfer study through porous fins (Si3N4 and AL) with temperature-dependent heat generation. Energy Convers. Manage. 74:9-16. http://dx.doi.org/10.1016/j.enconman.2013.04.034
Hatami M, Mehdizadeh Ahangar GHR, Ganji DD, Boubaker K (2014). Refrigeration efficiency analysis for fully wet semi-spherical porous fins. Energy Convers. Manage. 84:533-540. http://dx.doi.org/10.1016/j.enconman.2014.05.007
Joneidi AA, Ganji DD, Babaelahi M (2009). Differential transformation method to determine fin efficiency of convective straight fins with temperature dependent thermal conductivity. Int. Commun. Heat Mass Transf. 36(7):757-762. http://dx.doi.org/10.1016/j.icheatmasstransfer.2009.03.020
Kraus AD, Aziz A, Welty J (2001). Extended Surface Heat Transfer. Wiley. New York.
Lin WW, Lee DJ (1999). Boiling on a straight pin fin with variable thermal conductivity, Heat Mass Transf. 34(5):381-386. http://dx.doi.org/10.1007/s002310050273
Mills AF (1995). Basic heat and mass transfer. Irwin INC. Chicago.
Moradi A, Ahmadikia H (2010). Analytical solution for different profiles of fin with temperature dependent thermal conductivity. Math. Prob. Eng. 10:1-15. http://dx.doi.org/10.1155/2010/568263
Rajabi A (2007). Homotopy perturbation method for fin efficiency of convective straight fins with temperature-dependent thermal conductivity. Phys. Lett. A. 364(1):33-37. http://dx.doi.org/10.1016/j.physleta.2006.11.062
Rashidi MM, Laraqi N, Sadri SM (2010). A novel analytical solution of mixed convection about an inclined flat plate embedded in a porous medium using the DTM-Padé. Int. J. Therm. Sci. 49(12):2405-2412. http://dx.doi.org/10.1016/j.ijthermalsci.2010.07.005
Sharqawy MH, Zubair SM (2007). Efficiency and optimization of an annular fin with combined heat and mass transfer-an analytical solution. Int. J. Refrig. 30(5):751-757. http://dx.doi.org/10.1016/j.ijrefrig.2006.12.008
Unal HC (1987). An analytical study of boiling heat transfer from a fin. Int. J. Heat Mass Transf. 30(2):341-349. http://dx.doi.org/10.1016/0017-9310(87)90122-0
Zhou JK (1986). Differential transformation method and its application for electrical circuits. Wuhan (China), Hauzhang University press.

academicJournals

Vol. 9(21), pp. 475-486, 16 November, 2014
DOI: 10.5897/IJPS2014.4202
Article Number: 0AF078548551
ISSN 1992 - 1950

http://www.academicjournals.org/IJPS

International Journal of Physical Sciences

Full Length Research Paper

Estimation of heavy metals contamination and silicate mineral distributions in suspended sediments of Subansiri River

B. J. Saikia[1], S. R. Goswami[2] and R. R. Borah[3]

[1]Department of Physics, Anandraram Dhekial Phookan College, Nagaon 782 002, India.
[2]Department of Physics, Assam Down Town University, Guwahati 781 026, India.
[3]Department of Physics, Nowgong College, Nagaon 782 001, India.

Received 31 August, 2014; Accepted 21 October, 2014

Suspended sediments samples were collected from ten different locations through the Subansiri River to assess heavy metals contamination such as Fe, Al, Ti, Pb, Zn, Cu, Ni, Co, Mn and Cr. The enrichment factor (EF), contamination factor (CF), geo-accumulation index (I_{geo}) and pollution load index (PLI) were investigated for evaluate metal contamination in the sediments. The relative distribution of major minerals such as quartz, feldspar (orthoclase and microcline) and kaolinite are determined by calculating extinction co-efficient. The mean concentration exhibits positive correlations among Fe, Al, Ti, Mn, Zn, Pb, Ni, and Co. The relative distributions of the contamination are: Al > Ti > Fe > Mn > Cu > Cr > Zn > Pb > Ni > Co. The investigating factors suggest the significant contamination for Subansiri river sediments are Cu and Pb. The mean concentrations of heavy metals in the sediments were found to be below the geochemical background level of world surface rock average. The elemental correlation is indicative to the metamorphosed pyrophanite ($MnTiO_3$) deposition. The infrared analysis indicates presence of micro-crystalline quartz particles and weathered metamorphous silicate minerals.

Key words: Heavy metals, suspended sediments, pollution.

INTRODUCTION

Sediments are detrital products of rocks and bear the mineralogical properties of the original rock formation. Geochemical studies of sediments are helpful in understanding the different sediment sources, element distribution pattern and evaluating the environmental conditions existing in an area. The mineralogical properties of sediments reflect the geological history of transport and sorting process. The sediments have been contaminated by heavy metals when rocks are disintegrated through natural and anthropogenic process. The accumulation and distribution of heavy metals are the most common environmental pollutants, and their occurrence in waters and biota indicate the presence of natural or anthropogenic sources (Cataldo et al., 2001; Hobbelen et al., 2004; Koukal et al., 2004; Okafor and Opuene, 2007; Mohiuddin et al., 2010). River sediments act as both source and sink for heavy metals. Many heavy metals such as Fe, Co, Cr, Mn, Ni, Zn, Cu, and Se

*Corresponding author. E-mail: vaskar_r@rediffmail.com

are essential elements for normal growth of plants and living organisms. However, at high concentrations of these metals become toxic. The metals, such as Pb or Cr, may be tolerated by the ecosystem in low concentration, but become harmful in higher concentrations (Alloway and Ayres, 1997; Nriagu, 1988). Recently deposited trace elements in bed sediments can provide information on transport processes and sources. As deposition occurs over time that is, the deep sediments become a historical record of the temporal trends of chemicals in the environment. However, studies of river sediments especially big rivers and sedimentary rock geochemistry have made important contributions all over the world to interpret tectonic settings and estimates of average upper crustal composition.

Chemical weathering of rocks is one of the major processes which modify the Earth's surface. The heavy metals contaminations in river sediments has been studied by various authors in many rivers (Priju and Narayana, 2007; Nabi Bidhendi et al., 2007; Dixit and Tiwari, 2008; Mumba et al., 2008; Kashulin et al., 2008; Mensi et al., 2008; Akoto et al., 2008; Venugopal et al., 2009; Biati et al., 2010; Nouri et al., 2010; Buccolieri et al., 2006; Acevedo-Figueroa, 2006; Karbassi et al., 2007; Cuculic et al., 2009). The focus on mineralogical, geochemical and geophysical studies and chemical composition of sediments of many Indian rivers were done by Borole et al. (1982); Subramanian et al. (1985, 1987); Seralathan (1987); Ramesh et al. (1990); Chakrapani and Subramanian (1990); Singh et al. (1997); Kotoky et al. (1997); Singh (1999); Subramanian (1988); Dekov (1998); and Braun et al. (2009).

The variations in bulk rock composition or weatherable rocks can generate significant differences in dissolved chemical components. The dissolved chemical load and sediment flux of Brahmaputra river has significantly higher rates of physical and chemical weathering than other large Himalayan catchments (Sarin et al., 1989; Harris et al., 1998; Galy and France-Lanord, 1999; Galy and France-Lanord, 2001; Dalai et al., 2002; Singh and France-Lanord, 2002; Singh et al., 2005). The estimation of silicate distribution in sediments is important because the total CO_2 consumption by silicate weathering can be approximated by the total molar charge equivalents of all cations generated by silicate weathering. In many weathering environment, the chemical weathering of silicate minerals results in the formation of secondary clays.

Present study is confined in the river Subansiri, one of the most important sediment carrying tributary of Brahmaputra river. Subansiri river basin is influenced by two main tectonic features: main central thrust (MCT) and the main boundary thrust (MBT). The rock structure is fine grained to pebbly, weathered, highly jointed to massive sandstone, medium to coarse grained, soft weathered to shared, massive to moderately jointed sandstone with stringers of carbonaceous material. The overall rock composition is poor which causes more erosion in the basin. As river sediments act as both source and sink for heavy metals therefore contaminants may eventually pass through the food chain and result in a wide range of adverse environmental effects. This spectroscopic study is conducted to evaluate the concentration of heavy metals (Fe, Al, Ti, Pb, Zn, Cu, Ni, Co, Mn and Cr) due to the natural and anthropogenic activities of the river Subansiri, which helps to assess the ecotoxic potential of the river sediments.

MATERIALS AND METHODS

Sample collection and preparation

The suspended sediment samples were collected from ten locations of the Subansairi river (Figure 1). Suspended samples were collected at a depth of 2 to 3 ft. from the surface of each sampling locations. To eliminate the possibility of bank materials of the local origin, special care is taken on the sample collection by collecting them as far away from the banks as possible. The precise location (longitude and latitude) of the sampling sites has been determined using handheld Global Positioning System (GPS) (Table 1).

The suspended particles were separated by gravimetric method using Whatman filter paper (40 μ). The wet samples were allowed to dry and the moisture contents were removed by heating the samples at temperature 110°C for 10 min. The heavy metals (Al, Co, Cr, Cu, Fe, Mn, Ni, Pb, Ti and Zn) in sediment samples were determined using a Philips MagiX PRO wavelength dispersive X-ray spectrometer with a rhodium anode X-ray tube was used, which may operated at up to 60 kV and current up to 125 mA, at a maximum power level of 4 kW. The precision and accuracy of the data is ±2%, and average values of three replicates were taken for each determination. The powdered samples (0·25 g) were put into platinum crucibles and HNO_3 (conc.), HCl, H_2O_2 and HF were added in the proportion of 5: 2: 1: 2 ml. Crucibles were heated on hot plate and the solution evaporated to near dryness. After that, 2 ml HF were added few times until precipitate of SiO_2 was eliminated as SiF_4 vapours. After cooling down to room temperature, a mixture of HCl (conc.) and redistilled water at a ratio 2: 5 ml was added, the solution transferred in 50 ml volumetric flasks and filled up with redistilled water. Then 0·5 g of powdered sample was put in a glass beaker and a mixture of redistilled water and HCl (conc.) in a ratio 15: 20 ml was added and the solution evaporated to near dryness. The residue was dissolved with 10 ml 1% tin, and SiO_2 precipitated and coagulated. Precipitate was filtered and washed with HCl solution in a ratio of 5 : 95 ml. Filter paper and residue were transferred into a platinum crucible and heated at 1000°C for 10 min. Crucible was weighed and the content of SiO_2 calculated. The powdered sample was homogenized in spectrophotometric grade KBr (1: 20) in an agate mortar and was pressed with 3 mm pellets using a hand press. The infrared spectrum was acquired using Perkin-Elmer system 2000 FTIR spectrophotometer with helium–neon laser as the source reference, at a resolution of 4 cm^{-1}. The spectra were taken in transmission mode in the region 400 to 4000 cm^{-1}. The room temperature was 30°C during the experiment.

Extinction coefficient

To estimate the relative distribution of silicate minerals among the studied samples, the extinction coefficient for the characteristic peaks has been calculated. The extinction coefficient (*K*) has been

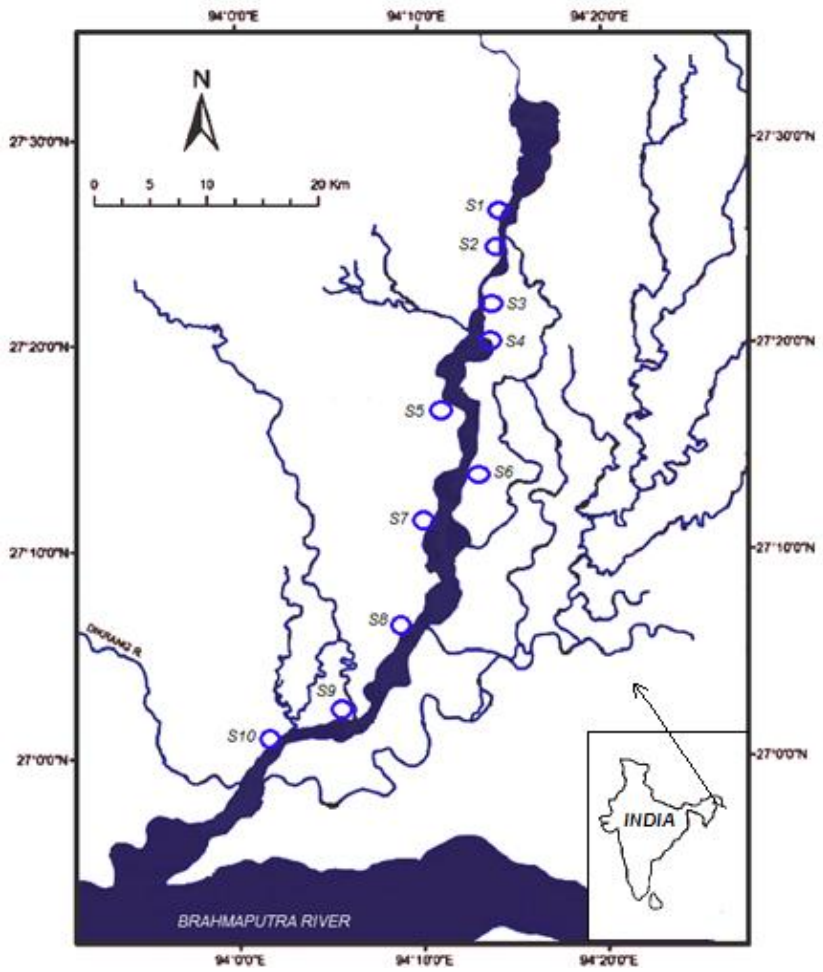

Figure 1. Sample collection sites of the Subansairi River.

Table 1. Location of sample collection

Site No.	Location	Latitude	Longitude	No. of Sample
S1	Pathalipum	27° 26' 59.03"N	94° 15' 12.49"E	3
S2	Lataijan	27° 25' 00.01"N	94° 14' 29.85"E	5
S3	Katari chapari	27° 23' 02.59"N	94° 13' 29.90"E	3
S4	Bhimpara Chapari	27° 20' 53.07"N	94° 13' 34.85"E	3
S5	Gohain	27° 18' 55.04"N	94° 11' 43.61"E	5
S6	Lakhimpur	27° 15' 42.27"N	94° 13' 03.33"E	7
S7	Mohaijan	27° 12' 42.59"N	94° 11' 39.90"E	5
S8	Ghagarmukh	27° 06' 27.59"N	94° 10' 00.41"E	7
S9	Mudoibil	27° 03' 13.92"N	94° 07' 34.56"E	3
S10	Baghor Deuri	27° 01' 16.13"N	94° 04' 42.15"E	5

calculated using the relation (Saikia et al., 2008):

$$K = \frac{DA}{m}$$

Where, *A* is the area of the pellet and *m* the mass of the sample.

The optical density (*D*) is defined as the logarithm to the base 10 of the reciprocal of the transmitted radiant power (*T*).

Index of geo-accumulation

The index of geo-accumulation (I_{geo}) is used to assess the

Table 2. Concentration of heavy metals in the Subansairi river sediments and world surface rock average.

Elements	Concentration of elements for site S1 to S10			World surface rock average*	Indian river sediment average**
	Min	Max	average ± standard deviation		
Fe	20850	30290	24527 ± 3187	35900	29000
Al	47060	59740	51456 ± 4477	69300	--
Ti	2210	3299	2762.90 ± 325	3800	--
Pb	11.80	39.50	23.92 ± 10	16	--
Zn	24.90	37.50	29.79 ± 5	127	16
Cu	74.10	198.25	129.19 ± 47	32	28
Ni	10.30	23.90	15.47 ± 5	49	37
Co	6.80	11.80	9.27 ± 1	13	--
Mn	582	685	626.50 ± 36	750	605
Cr	22.10	67.40	39.82 ± 16	71	87

Values are in ppm, *Martin and Meybeck (1979), **Subramaniam et al. (1987).

accumulation of contamination in sediments (Muller, 1969). The index of geo-accumulation is defined as:

$$I_{geo} = log_2 \frac{C_n}{1.5B_n}$$

Where, C_n is the measured concentration of element and B_n is the geochemical background value. The constant 1.5 allowed to analyze the possible natural fluctuations in background data due to lithologic effect. The seven grades or classes profile of the geo-accumulation index proposed by Muller (1981) and according to this classification the value of sediment quality is considered as unpolluted (I_{geo} is ≤ 0 , class 0); from unpolluted to moderately polluted (I_{geo} is 0-1 , class 1); moderately polluted (I_{geo} is 1-2 , class 2); from moderately to strongly polluted (I_{geo} is 2-3 , class 3); Strongly polluted (I_{geo} is 3-4 , class 4); from strongly to extremely polluted (I_{geo} is 4-5 , class 5) and Extremely polluted (I_{geo} is >6 , class 6). The total geo-accumulation index (I_{tot}) is defined as the sum of I_{geo} for all trace elements obtain from the site (Ya et al., 2007).

Enrichment factor

The contamination or enrichment factor (EF) is based on the standardization of the analysed element against a reference element. It is used to assess the level of contamination and the possible anthropogenic impact in sediments. The element which has low occurrence variability is considered as a reference element. Generally geochemical normalization of the heavy metals data to a conservative element, such as Al, Si and Fe is employed. In this study Fe is considered as reference element of normalization because natural sources (1.5%) vastly dominate its input (Tippie, 1984). The EF is defined as follows:

$$EF = \frac{C_{n(sample)}/C_{ref(sample)}}{B_{n(background)}/B_{ref(background)}}$$

Where, $C_{n(sample)}$ and $C_{ref(sample)}$ are the content of the examined and reference element in the examined environment respectively; $B_{n(background)}$ and $B_{ref(background)}$ are the content of examined and reference element in the reference environment respectively.

Due to the unavailability of metal background values for the study area, we used the values from world surface rocks (Martin and Meybeck, 1979) for analysis. We used categories of enrichment factor described by Mmolawa et al. (2011) that is, deficiency to minimal enrichment (EF < 2); moderate enrichment (2 ≤ EF < 5); significant enrichment (5 ≤ EF < 20); very high enrichment (20 ≤ EF < 40) and extremely high enrichment (EF ≥ 40) for our investigation.

Contamination factor (CF)

The level of contamination of sediment by metal is expressed in terms of CF calculated as:

$$CF = C_{Sample}/C_{Background}$$

Where, C_{Sample} is the concentration of the given metal in river sediment, and $C_{Background}$ is value of the metal equals to the world surface rock average given by Martin and Meybeck (1979). The CF and level of contamination proposed by Hakanson (1980) is used (Table 4) for describing the contamination level of this study. According to Hakanson the classifications are: low contamination (CF < 1); moderate contamination (1 ≤ CF < 3); considerable contamination (3 ≤ CF < 6) and very high contamination (CF > 6).

Pollution load index (PLI)

Pollution load index (PLI) for a particular site can be estimated using the method proposed by Tomilson et al. (1980).

$$PLI = (CF_1 \times CF_2 \times CF_3 \times \ldots\ldots\ldots \times CF_n)^{1/n}$$

Where, CF is the contamination factor and n is the number of metals.

RESULTS AND DISCUSSION

Metal contaminations

The concentration of heavy metals in the sediment samples of Subansairi river is presented in the Table 2. The enrichment factor (EF), contamination factor (CF), geo-accumulation index (I_{geo}), and pollution load index (PLI) of the studied samples were depicted in Tables 4, 5, 6, and 7 respectively. The world surface rock average

Table 3. Pearson's correlation coefficient between the heavy metal elements of the Subansairi river sediments.

Elements	Fe	Al	Ti	Pb	Zn	Cu	Ni	Co	Mn	Cr
Fe	1.00									
Al	**0.98**	1.00								
Ti	**0.99**	**0.98**	1.00							
Pb	-0.73	-0.81	-0.74	1.00						
Zn	-0.85	-0.90	-0.87	**0.96**	1.00					
Cu	0.48	0.33	0.43	0.10	-0.12	1.00				
Ni	-0.86	-0.90	-0.87	**0.96**	**1.00**	-0.12	1.00			
Co	-0.91	-0.96	-0.92	**0.94**	**0.98**	-0.16	**0.99**	1.00		
Mn	**0.88**	**0.91**	**0.89**	-0.92	-0.98	0.16	-0.98	-0.98	1.00	
Cr	-0.48	-0.58	-0.50	**0.93**	0.85	0.33	0.85	0.78	-0.81	1.00

Marked correlations are significant at $p < 0.05$.

prescribed by Martin and Meybeck (1979) is used as background value for investigation.

The concentration of Pb and Cu varied from 11.8 to 39.5 ppm with mean value 23.92 ppm, and 74.1 to 198.25 ppm with mean value 129.19 ppm respectively. This value is more than the world surface rock average as background level. The elements Pb and Fe expressed a strong positive correlation with Ni, Co, Cr and Al, Ti, Mn respectively at 0.05 level. The other elements such as Al have strong positive correlation with Ti and Mn; Ti has strong positive correlation with Mn; Zn has strong positive correlation with Co and Cr; Ni has strong positive correlation with Co and Cr at this level of significance (Table 3). The strong correlation indicates that these elements have common sources.

The EF values for Cu in Subansairi River sediments were ranged from 3.8574 to 8.3179. The EF values for Cu were found to be greater than 4 in most of sampling sites (Table 4), suggesting that these sites are classified as moderate enrichment for Cu. The stations S5, S6 and S7 are significant enrichment for Cu. In case of Pb, the EF values were ranged from 1.4410 to 2.9239. The sites S4 and S6-S10 are found to be moderate enrichment for Pb. The CF values for Cu in Subansairi River sediments varied from 2.6000 to 6.1953 with a mean value of 4.0370. For Pb the CF varies from 0.7375 to 2.4686 with a mean value of 1.495 (Table 5). Most sampling sites had the CF greater than 1 and less than 6 for the elements Cu and Pb. The remaining elements had the CF values less than 1. It was found that most sampling sites S4 - S10 were moderately contaminated by Pb. It was found that most sampling sites S1,S5,S6, S8,S9 and S10 face considerable contaminated by Cu except S2, S3, S4 were moderately contaminated. The site S7 has very high contamination of Cu. The I_{geo} values of majority elements in sampling sites were less than 0 (<0), except the elements Cu and Pb. The Igeo values of Cu and Pb in sites S2- S4 and S6-S10 were less than 1 (<1) respectively, in case of Cu the I_{geo} values of sampling sites S1, and S5-S10 were greater than 1 (>1) (Table 6). According to Muller's classification, the calculated I_{geo} values for Pb indicate sediment quality be considered as unpolluted to moderately polluted for S6- S10. The calculated Igeo values of Cu indicates sediment quality be considered as polluted for majority of sites as unpolluted and moderately polluted except the site S7 shows from moderately to strongly polluted.

The concentration of Fe in Subansairi River sediments varied from 20850 ppm at S1 to 30290 ppm at S7 with mean value 24527 ppm. The Fe mean value was less than world surface rock average as geochemical background level (Table 2). The CF values for Fe are ranged from 0.5808 at S1 to 0.8437 at S7, with a mean value of 0.6832. Because of the CF values for Fe in all sampling sites less than 1, Subansiri River Sediments face low contamination by Fe. The I_{geo} values for Fe at all sampling sites were negative. According to Muller's classification, Subansiri river sediments were unpolluted by Fe.

Zn concentration ranged between 24.9 and 37.5 ppm with mean value 29.79 ppm. The mean value is less than the world surface rock average as a geochemical background level (Table 2). Zn expressed very strong positive correlation with Ni and strong positive correlation with Co and Cr at 0.05 level. The highest values of Zn concentration is reported at S7. The concentration of Zn at all sampling sites were found to be below the geochemical background level of world surface rock average.

The enrichment factor (EF) values for Zn in Subansiri River sediments ranged from 0.2777 at S6 to 0.4013 at S1. The EF values for majority of sampling sites were greater than 0.3 and less than 0.4 (Table 4), suggesting that these sites are classified as deficiency to minimal enrichment for Zn. The CF values for Zn are varied from 0.2331 at S1 and 0.2528 at S10 with mean value of 0.2346 (Table 5). All sampling sites have CF less than 1, therefore, all sampling sites were classified as low contaminated. The I_{geo} values for Zn in all sampling sites were less than 0 (<0) (Table 6). These negative values indicate that the Subansiri River sediments in the study area are unpolluted by Zn.

Table 4. Enrichment ratio (ER) values of heavy metals in Subansiri river sediments.

Elements	Sample sites									
	S1	S2	S3	S4	S5	S6	S7	S8	S9	S10
Al	1.1866	1.1831	1.1307	1.0665	1.0392	1.0173	1.0217	1.0005	1.1350	1.1528
Ti	1.0014	1.1128	1.0604	1.1393	1.0438	1.0850	1.0289	1.0070	1.0994	1.0837
Pb	1.4410	1.2617	1.5183	2.2548	1.5698	2.7341	2.9239	2.8694	2.4653	2.1903
Zn	0.4013	0.3707	0.3566	0.3113	0.2872	0.2777	0.3499	0.3490	0.3732	0.3678
Cu	5.2430	4.4530	3.8574	4.2753	7.8986	8.3179	7.3456	6.4847	5.2424	4.8133
Ni	0.3900	0.3913	0.4587	0.4082	0.3587	0.2978	0.5781	0.5383	0.5997	0.5375
Co	0.9009	1.1461	1.2172	1.0222	1.1403	1.0465	1.0762	0.8767	1.0088	1.0414
Mn	0.1515	0.1486	0.1414	0.1352	0.1141	0.1294	0.0994	0.0989	0.1122	0.1129
Cr	0.5456	0.5810	0.5182	0.5745	0.7386	0.8619	1.1250	1.0427	0.9880	0.9878

Table 5. Contamination factor (CF) values of heavy metals in Subansiri river sediments.

Elements	Sample sites									
	S1	S2	S3	S4	S5	S6	S7	S8	S9	S10
Fe	0.5808	0.5841	0.6006	0.6398	0.6883	0.7059	0.8437	0.8075	0.6941	0.6871
Al	0.6892	0.6911	0.6791	0.6824	0.7153	0.7180	0.8620	0.8079	0.7879	0.7922
Ti	0.5816	0.6500	0.6368	0.7289	0.7184	0.7658	0.8682	0.8132	0.7632	0.7447
Pb	0.8375	0.7375	0.9125	1.4438	1.0813	1.9313	2.4688	2.3188	1.7125	1.5063
Zn	0.2331	0.2165	0.2142	0.1992	0.1976	0.1961	0.2953	0.2819	0.2591	0.2528
Cu	3.0438	2.6000	2.3156	2.7344	5.4344	5.8688	6.1953	5.2344	3.6375	3.3063
Ni	0.2265	0.2286	0.2755	0.2612	0.2469	0.2102	0.4878	0.4347	0.4163	0.3694
Co	0.5231	0.6692	0.7308	0.6538	0.7846	0.7385	0.9077	0.7077	0.7000	0.7154
Mn	0.8800	0.8680	0.8493	0.8653	0.7853	0.9133	0.8387	0.7987	0.7787	0.7760
Cr	0.3169	0.3394	0.3113	0.3676	0.5085	0.6085	0.9493	0.8423	0.6859	0.6789

The concentration of Ni value was between 10.3 and 23.9 ppm with mean concentration 15.47 ppm. The mean value is less than the world surface rock average as background level. Ni concentrations of Subansiri River sediments vary between 10.3 ppm at S6 and 23.9 ppm at S7. The EF values for Ni are range from 0.2978 at S6 to 0.5997 at S9 (Table 4). The EF values for all sampling sites were less than 0.6, suggesting that these sites are classified as deficiency to minimal enrichment for Ni. The CF values for Ni are ranged from 0.2102 at S6 to 0.4878 at S7, with mean value of 0.3157. These values of CF represent the sampling sites as low contaminated. The I_{geo} values for Ni at all sampling sites were negative. According to Muller's classification, Subansiri River sediments were unpolluted at all sites due to Ni.

Co concentration ranged between 6.8 and 11.8 ppm with mean value 28.16 and 9.27 ppm. The mean value of Co concentration is less than the

Table 6. Geo-accumulation index (I_{geo}) values of heavy metals in Subansiri river sediments.

Elements	Sample sites									
	S1	S2	S3	S4	S5	S6	S7	S8	S9	S10
Fe	-1.3689	-1.3606	-1.3206	-1.2292	-1.1239	-1.0875	-0.8301	-0.8934	-1.1116	-1.1262
Al	-1.1220	-1.1181	-1.1433	-1.1363	-1.0684	-1.0628	-0.7991	-0.8927	-0.9289	-0.9210
Ti	-1.3669	-1.2065	-1.2359	-1.0411	-1.0621	-0.9699	-0.7889	-0.8834	-0.9749	-1.0102
Pb	-0.8408	-1.0243	-0.7171	-0.0551	-0.4723	0.3646	0.7188	0.6284	0.1911	0.0060
Zn	-2.6861	-2.7923	-2.8081	-2.9126	-2.9240	-2.9356	-2.3448	-2.4118	-2.5336	-2.5692
Cu	1.02089	0.7935	0.6264	0.8662	1.8572	1.9680	2.0462	1.8031	1.2780	1.1402
Ni	-2.7272	-2.7143	-2.4448	-2.5216	-2.6027	-2.8351	-1.6207	-1.7869	-1.8492	-2.0211
Co	-1.5199	-1.1644	-1.0375	-1.1979	-0.9349	-1.0224	-0.7247	-1.0838	-1.0995	-1.0682
Mn	-0.7694	-0.7892	-0.8206	-0.7936	-0.9336	-0.7158	-0.8388	-0.9093	-0.9459	-0.9508
Cr	-2.2427	-2.1438	-2.2688	-2.0287	-1.5608	-1.3018	-0.6600	-0.8326	-1.1289	-1.1438

Table 7. Pollution load index (PLI) values of heavy metals in Subansiri river sediments.

Values	Sample sites										Mean
	S1	S2	S3	S4	S5	S6	S7	S8	S9	S10	
PLI	0.5834	0.5876	0.6020	0.6507	0.7083	0.7712	1.0005	0.9067	0.7981	0.7676	0.7376

world surface rock average as geochemical background level. Co showed good positive correlation with Cr at 0.05 level. The EF values for Co are ranged from 0.8767 at S8 and 1.1461 at S2 (Table 4). The EF values of sampling sites suggesting that these sites are classified as deficiency to minimal enrichment for Co. All sampling sites have CF less than 1, therefore, all sampling sites were classified as low contaminated. The negative value of I_{geo} at all sampling sites represents Muller's classification as unpolluted at all sites due to Co.

Mn concentration ranged between 582 ppm at S10 and 685 ppm at S6 with mean value 626.5 ppm. The mean value of Mn was less than world surface rock average as geochemical background level. The EF values for all sampling sites (Table 4), suggesting that these sites are classified as deficiency to minimal enrichment for Mn. The contamination factor (CF) values for Mn are varied from 0.7760 at S10 to 0.9133 at S6 (Table 5). The values of CF suggest the sampling sites were low contaminated. According to Muller's classification, the negative I_{geo} values for Mn at all sampling sites represents sediments are unpolluted by Mn.

Cr concentration varied between 22.1 ppm at S3 and 67.4 ppm at S7 with mean value 39.82 ppm. It was less than world surface rock average as geochemical background level, (Table 2). The EF values for Cr in all sampling sites are classified as deficiency to minimal enrichment for Cr. The I_{geo} values for Cr at all sampling sites were negative. According to Muller's classification, Subansiri river sediments were unpolluted by Cr. The contaminations of various sampling sites were compared by determining the PLI. PLI values of the analyzed samples ranged from 0.5834 at S1 to 1.0005 at S7 with a mean value of 0.7376 (Table 7). All sampling sites suggest has no overall pollution, whereas S7 shows signs of pollution.

The very strong positive correlation of Al with Fe (0.98) indicates their association with clay derived from the adjoin study sites. A very strong positive correlation of Al (0.98) and Fe (0.99) with Ti is observed, but, generally Ti shows a strong correlation with Al or Fe in the marine sediments. The manganese titanium oxide mineral Pyrophanite

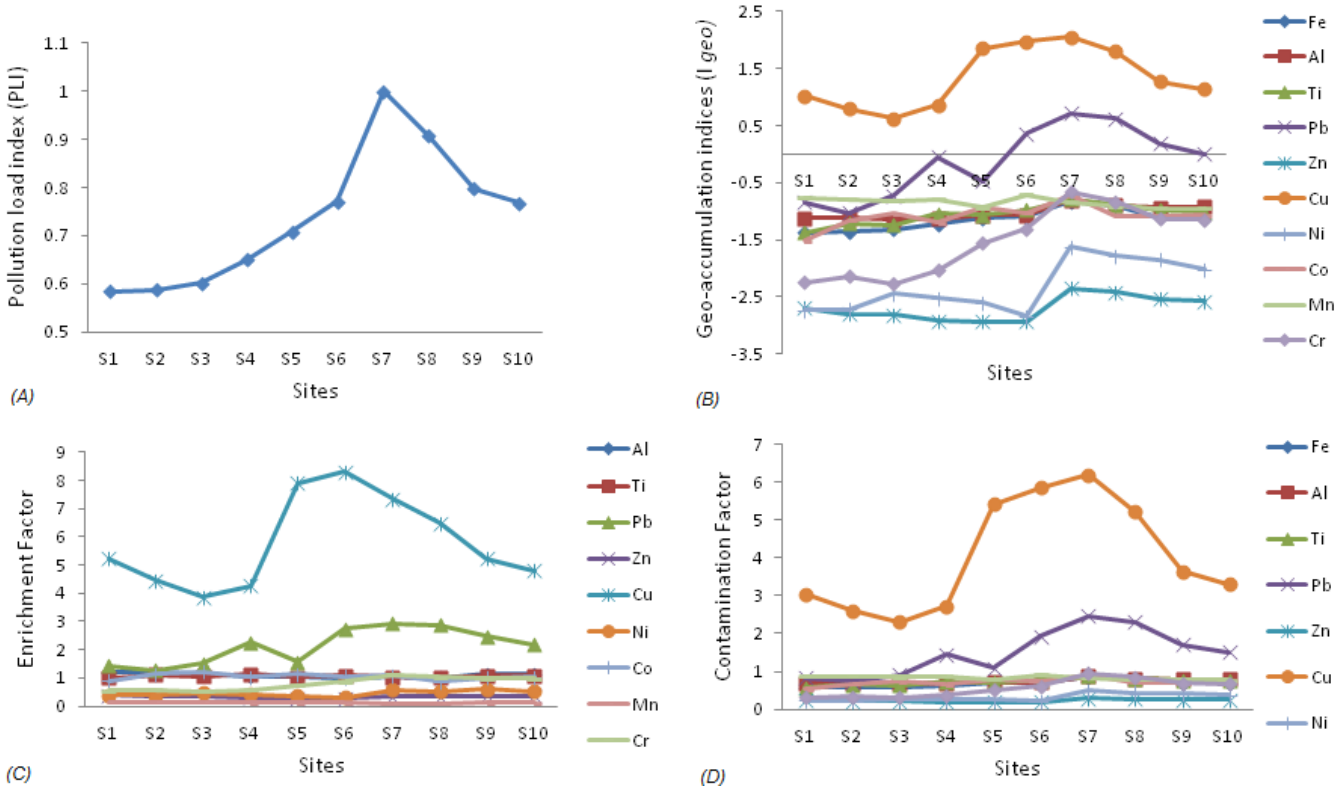

Figure 2. (*A*) Pollution load index values, (*B*), Geo-accumulation indices (I_{geo}), (*C*) Enrichment Factor (EF) of heavy metals, (*D*) Contamination factor (CF) of heavy metals of sampling sites at Subansiri River.

($MnTiO_3$) is usually found in metamorphosed manganese deposits. Therefore, the observed positive correlation between Ti and Mn may indicative to the presence of pyrophanite mineral deposition in the adjoin areas of the study sites.

Figure 2A is corresponding to the pollution load indices of the sampling sites. The pollution load indices provide a comparative assessment of the site quality. According to Tomlinson et al. (1980) assessment, when the value of pollution load indices is < 1 then the site has perfection but, the value > 1 would indicate deterioration of site quality. The value of pollution load indices is equal to 1 indicates that only baseline levels of pollutants are present. Among the sampling sites, in the site S7 the value of pollution load indices is found to be slightly greater than 1, which is indicative to the deterioration of sediment quality in the sites. The growth of the industries in the adjacent areas of this site cannot be ignored for it. Chakravarty and Patgiri (2009) has also reported the nature of pollution in the adjacent area of this site.

The very strong positive correlation of Al with Fe (0.98) indicates their association with clay derived from the adjoin study sites. A very strong positive correlation of Al (0.98) and Fe (0.99) with Ti is observed, but, generally Ti shows a strong correlation with Al or Fe in the marine sediments. The manganese titanium oxide mineral Pyrophanite ($MnTiO_3$) is usually found in metamorphosed manganese deposits. Therefore, the observed positive correlation between Ti and Mn may indicative to the presence of pyrophanite mineral deposition in the adjoin areas of the study sites.

The geo-accumulation index (I_{geo}) is used to determine the pollution level of sediments. Figure 2B indicates that the calculated I_{geo} values of heavy metal Cu in the sampling sites S5- S10 have the Muller's class 2. The I_{geo} values of Pb in the sampling sites S7 and S8 indicates the Muller's class 1, whereas the other investigated heavy metals in the sampling sites exhibit the Muller's class 0. This indicates that Cu and Pb are responsible for pollution of the respective sites. The Pb pollution of the adjacent area of the site S7 has also reported by the previous worker Chakravarty and Patgiri (2009).

Figure 2C depicts the enrichment factor of the heavy metals in the sampling sites. The significant enrichment of Al in the sites S1 and S5-S9 and a moderate enrichment of Pb in the sites S4 and S6-S10 is observed. The heavy metals in other sites have the permissible categories of enrichment values as reported in by Mmolawa et al. (2011). The contaminations of the heavy metals in the sampling sites are presented in Figure 2D. The sites S1 and S5-S10 are considerably contaminated

Table 8. The observed absorption wave numbers and corresponding silicate minerals from FTIR spectra in different sites of the Subansiri river sediments

S/ No.	Mineral	Sample Sites	Observed Wave numbers (cm^{-1})
1	Quartz	S1-S10	460-467
		S1-S10	520-524
		S1-S10	691-697
		S1-S10	7776-781
		S1-S10	1080-1082
		S1-S10	1164-1178
		S1-S4, S7-S10	1612-1622
2	Orthoclase (Feldsper)	S1-S10	530-535
		S1-S10	644-649
3	Microcline (Feldsper)	S1-S10	580-585
4	Kaolinite	S1-S4, S8-S10	1011-1019
		S6-S10	1032-1039
		S1-S4, S6-S7	3616-3621
		S5, S8-S10	3691-3692

by Cu and sites S4-S10 are moderately contaminated due to Pb according to the level of contamination as suggested by Hakanson (1980). The heavy metals in other sites have below contamination level. The comparison of the Indian river sediment average (Table 2), the Subansiri river is contaminated by heavy metals Zn, Cu and Mn. It is worthwhile that the value of Pb is much higher than the world surface rock average. Therefore, the Subansiri river is contaminated by Cu, Pb, Zn and Mn and the significant heavy metal pollutant of this river is Cu.

Distribution of silicate minerals

The observed infrared frequencies of the studied sediment samples were compared with the available literature of Gadsden (1975) and the minerals such as quartz, microcline feldspar, orthoclase feldspar, kaolinite, are identified. The observed frequencies are interpreted in Table 8. The mid infrared spectra of silicate in between the range 1200 to 400 cm^{-1} are generally classified into characteristic region or fingerprint region. In this characteristic region, the octahedral peak at 695 cm^{-1} is unique to the crystalline quartz (Saikia et al., 2008). All studied samples exhibits peaks at around 695cm^{-1} which indicative of the presence of micro-crystalline quartz particles. In the fingerprint region, the characteristic peaks of quartz, orthoclase, microcline and kaolinite at around 778 647, 585 and 1019 cm^{-1} respectively are taken for estimation of extinction coefficient.

The absorption peaks at 1615 to1620 cm^{-1} indicates the presence of quartz in river sediments are weathered from metamorphic origin (Keller and Pickett, 1949). The discussion of Ramasamy et al. (2004, 2005, 2006). also indicates to the presence of silicates at this range in river sediments from the weathered metamorphic rocks (Ramasamy et al., 2004, 2005, 2006). The presence of absorption peaks in between 1612 to 1622 cm^{-1} in this study is indicative to the origin of the observed silicate minerals.

The calculated extinction co-efficient values of quartz are greater than other silicate minerals in all the sites. Therefore, microcrystalline quartz particles is the major constitutes in all study sites. It throws light on the nature of erosion and environmental degradation. The maximum extinction co-efficient values for quartz, orthoclase, microcline and kaolinite are 156.91, 28.451, 53.171 and 15.921 in the site no. S1, S8, S4 and S1 respectively, whereas the minimum values are 113.531, 9.891, 22.76 and 4.83 in the site no. S5, S4, S6 and S4 respectively (Table 9). This observed range of extinction coefficient values of the silicate minerals in the study sites indicates a low fluctuation of distribution. The distribution of kaolinite is very much lesser than quartz and feldspar in the study sites (Figure 3).

Conclusion

The investigation of Subansiri River sediments shows the order of the mean concentrations of tested heavy metals as: Al > Ti > Fe > Mn > Cu > Cr > Zn > Pb > Ni > Co. The correlation analysis of mean concentrations showed good to strong positive correlations among Fe, Al, Ti, Mn, Zn, Pb, Ni, and Co, suggesting that these metals have common sources. The EF, CF, geo-accumulation index (I_{geo}) and PLI were applied for assessment of contamination. The EF values suggest that Subansiri river sediments were moderate enriched for Cu and Pb. The CF values suggest that sample sites are moderate contaminated by Cu and some sites suffers low

Table 9. Observed values of extinction-coefficients of Quartz, Orthoclase, Microcline, and Kaolinite minerals in different sites of the Subansiri river sediments using FT-IR analysis

Sample Sites	Peak intensity (Å)				Extinction coefficient			
	778 cm^{-1} (Quartz)	647 cm^{-1} (Orthoclase)	585 cm^{-1} (Microcline)	1019 cm^{-1} (Kaolinite)	Quartz	Orthoclase	Microcline	Kaolinite
S1	0.9974	0.1104	0.1704	0.1012	156.96	17.37	26.80	15.92
S2	0.8874	0.1007	0.3071	0.0632	139.60	15.84	48.31	9.95
S3	0.7693	0.1648	0.1978	0.0475	121.02	25.93	31.12	7.48
S4	0.8874	0.0629	0.3380	0.0307	139.60	9.89	53.17	4.83
S5	0.7217	0.0959	0.2471	0.0588	113.53	15.09	38.87	9.26
S6	0.9278	0.1585	0.1447	0.0686	145.95	24.93	22.76	10.79
S7	0.8595	0.1149	0.2229	0.0543	135.21	18.08	35.07	8.55
S8	0.8371	0.1809	0.2297	0.0422	131.69	28.46	36.13	6.64
S9	0.8969	0.0991	0.2005	0.0557	141.09	15.60	31.54	8.76
S10	0.9602	0.1725	0.1481	0.0456	151.05	27.14	23.29	7.18

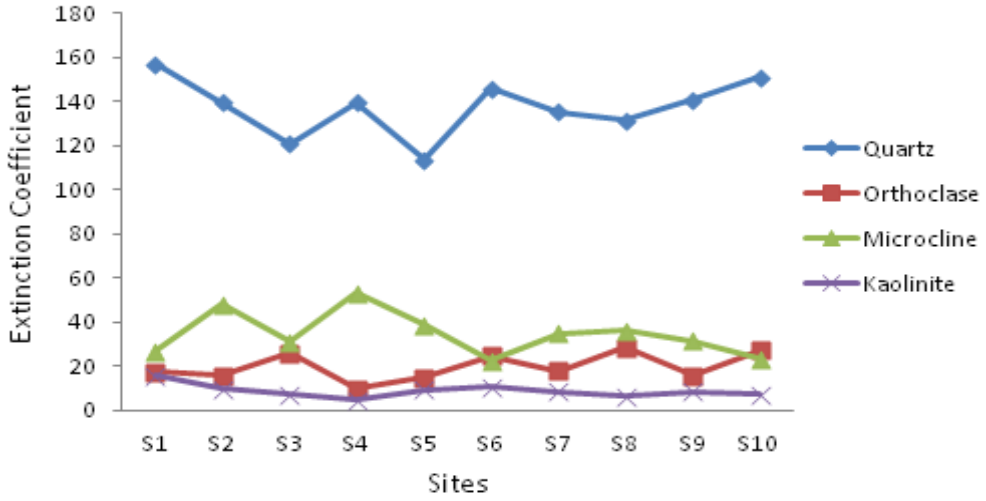

Figure 3. The relative distribution pattern of Quartz, Orthoclase, Microcline, and Kaolinite minerals in different sites of the Subansiri river sediments.

contamination due to Pb. The I_{geo} values show that the sediments quality is moderately polluted for Cu and from unpolluted to moderately polluted for Pb. PLI of all sites suggest sampling sites suggest has no overall pollution, only site S7 shows signs of pollution. The negative value of I_{tot} indicates that the mean concentrations of heavy metals Subansiri river sediments are lower than world surface rock average.

It is worthwhile to mention that in the site S1 there is absence of industrial establishments, but we observed the effects of heavy metal Cu in this area. On the other hand, the heavy metals Cu, Ni, Pb and Zn have been reported by Geological Survey of India in 1974 and 1983 (GSI, 1974 and GSI, 1983) from the metamorphic belt lying in the Subansiri river catchment. Therefore, the sediment is contaminated with Cu and Pb that is due to dispersion from the mineralized zone of the upper catchment area. But the effects of anthropogenic factors cannot be ignored due to the gradually developing industries and habitats (for example site S7) in the adjacent areas of the sampling locations. The very strong positive correlations of Al with Fe are indicative to their association with clay. The observed positive correlation between Ti and Mn is indicative to the presence of pyrophanite ($MnTiO_3$) mineral from the metamorphosed manganese deposition in the adjoin areas.

The infrared analysis of the Subansiri River sediments indicates the presences of quartz, feldspar (orthoclase and microcline) and kaolinite as major minerals. The presence of absorption peaks in between 1612 to 1622 cm^{-1} in this study is indicative to the weathered metamorphic origin of the silicate minerals. All studied samples exhibits peaks at around 695 cm^{-1} which indicative to the presence of micro-crystalline quartz

particles in the sediment samples. The range of extinction coefficient of the silicate minerals in the study sites has a low fluctuation of distribution. The quartz exhibits higher extinction co-efficient values than all other silicate minerals; therefore, it throws light on the nature of erosion and environmental degradation.

Conflict of Interest

The authors have not declared any conflict of interest.

ACKNOWLEDGEMENTS

Authors thank the Directors, National Geophysical Research Institute (NGRI-CSIR), Hyderabad and North East Institute of Science and Technology (NEIST-CSIR), Jorhat for their cooperation during this work. They also thank Dr. J.R. Chetia, Dibrugarh University, Dibrugarh, for his assistance in the FTIR analysis.

REFERENCES

Acevedo-Figueroa D (2006). Trace metals in sediments of two estuarine lagoons from Puerto Rico. Environ. Poll. 141(2):336-342. http://dx.doi.org/10.1016/j.envpol.2005.08.037

Akoto O, Ephraim JH, Darko G (2008). Heavy metals pollution in surface soils in the vicinity of abundant railway servicing workshop in Kumasi, Ghana. Int. J. Environ. Res. 2(4):359-364.

Alloway BJ, Ayres DC (1997). Chemical principles of environmental pollution, second edition, Blackie Academic and Professional, Chapman and Hall, London. pp. 208-211.

Biati A, Moattar F, Karbassi AR, Hassani AH (2010). Role of saline water in removal of heavy elements from industrial wastewaters. Int. J. Environ. Res. 4(1):177-182.

Borole DV, Sarin MM, Somayajulu BLK (1982). Composition of Narmada and Tapti Estuarine particles and adjacent Arabian sea sediments. Ind. J. Mar. Sci. 11:51-62.

Braun JJ, Descloîtres M, Riotte J, Fleury S, Barbiero L, Boeglin J, Violette A, Lacarce E, Ruiz L, Sekhar M, Kumar MSM, Subramanian S, Dupré B (2009). Regolith mass balance inferred from combined mineralogical, geochemical and geophysical studies: Mule Hole gneissic watershed, South India. Geochem. Cosmochim. Acta 73(4):935-961. http://dx.doi.org/10.1016/j.gca.2008.11.013

Buccolieri A, Buccolieri G, Cardellicchio N, Dell'Atti A, Di Leo A, Maci A (2006). Heavy metals in marine sediments of Taranto Gulf (Ionian Sea, Southern Italy). Marine Chem. J. 99:227–235. http://dx.doi.org/10.1016/j.marchem.2005.09.009

Cataldo D, Colombo JC, Boltovskoy D, Bilos C, Landoni P (2001). Environmental toxicity assessment in the Parana river delta (Argentina): simultaneous evaluation of selected pollutants and mortality rates of *Corbicula Fluminea (Bivalvia)* early juveniles. Environ. Poll. 112(3):379-389. http://dx.doi.org/10.1016/S0269-7491(00)00145-7

Chakrapani GJ, Subramanian V (1990). Preliminary studies on the geochemistry of the Mahanadi river basin, India. Chem. Geol. 70:247-266.

Chakravarty M, Patgiri AD (2009). Metal pollution assessment in sediments of the Dikrong River, N.E. India. J. Hum. Ecol. 27(1):63-67.

Cuculic V, Cukrov N, Kwokal Z, Mlakar M (2009). Natural and anthropogenic sources of Hg, Cd, Pb, Cu and Zn in seawater and sediment of Mljet National Park, Croatia Estuarine. Coastal Shelf Sci. J. 81:311-320 http://dx.doi.org/10.1016/j.ecss.2008.11.006

Dalai TK, Krishnaswami S, Sarin MM (2002). Major ion chemistry in the headwaters of the Yamuna river system: Chemical weathering, its temperature dependence and CO_2 consumption in the Himalaya. Geochim. Cosmochim. Acta. 66:3397-3416. http://dx.doi.org/10.1016/S0016-7037(02)00937-7

Dekov VM (1998). Chemical composition of sediments and suspended matter from the Cauvery and Brahmaputra rivers (India). Sci. Total Environ. 212(2-3):89-105. http://dx.doi.org/10.1016/S0048-9697(97)00132-0

Dixit S, Tiwari S (2008). Impact assessment of heavy metal pollution of Shahpura Lake, Bhopal, India. Int. J. Environ. Res. 2(1):37-42.

Gadsden JA (1975). Infrared Spectra of Minerals and Related Inorganic compounds, Butterworths. USA. pp. 189-235.

Galy A, France-Lanord C (1999). Weathering processes in the Ganges–Brahmaputra basin and the riverine alkalinity budget. Chem. Geol. 159:31-60. http://dx.doi.org/10.1016/S0009-2541(99)00033-9

Galy A, France-Lanord C (2001). Higher erosion rates in the Himalaya: geochemical constraints on riverine fluxes. Geology 29:23–26. http://dx.doi.org/10.1130/0091-7613(2001)029<0023:HERITH>2.0.CO;2

GSI (1974). Geology and Mineral Resources of the States of India (Part IV–Arunachal Pradesh, Assam, Manipur, Mizoram, Nagaland and Tripura). Geol Sur of India Misc Pub No. 30, Kolkata: GSI.

GSI (1983). Proceedings of the symposium on geology and mineral resources of North Eastern Himalayas. Geol. Surv. India Misc Pub No. 43, Kolkata: GSI.

Hakanson L (1980). An ecological risk index for aquatic pollution control a sedimentological approaches. Water Res. 14(8):975-1001. http://dx.doi.org/10.1016/0043-1354(80)90143-8

Harris N, Bickle MJ, Chapman H, Fairchild I, Bunbury J (1998). The significance of Himalayan rivers for silicate weathering rates: Evidence from the Bhote Kosi tributary. Chem. Geol. 144:205–220. http://dx.doi.org/10.1016/S0009-2541(97)00132-0

Hobbelen PHF, Koolhaas JE, van Gestel CAM (2004). Risk assessment of heavy metal pollution for detritivores in floodplain soils in the Biesbosch, The Netherlands, taking bioavailability into account. Environ. Poll. 129 (3):409-419. http://dx.doi.org/10.1016/j.envpol.2003.11.010

Karbassi AR, Monavari SM, Nabi Bidhendi Gh R, Nouri J, Nematpour K (2008). Metal pollution assessment of sediment and water in the Shur River. Environ. Monit. Assess. J. 147:107-116. http://dx.doi.org/10.1007/s10661-007-0102-8

Kashulin NA, Terentiev PM, Koroleva IM (2008). The status of whitefish population from Chuna Lake in the Lapland Biosphere Reserve Russia. Int. J. Environ. Res. 2(2):111-124.

Keller WD, Pickett EE (1949). Absorption of infrared radiation by powdered silica minerals. The American mineralogist. 34:855-868.

Kotoky P, Baruah J, Baruah NK, Sarma JN (1997). Geoenvironmental studies of the river Jhanji, Assam. J. Hum. Ecol. Special Issue No. 6: 55-67.

Koukal B, Dominik J, Vignati. D, Arpagaus P, Santiago S, Ouddane B, Benaabidate L (2004). Assessment of water quality and toxicity of polluted rivers Fez and Sebou in the region of Fez (Morocco). Environ. Poll. 131(1):163-172. http://dx.doi.org/10.1016/j.envpol.2004.01.014

Martin JM, Meybeck M (1979). Elemental mass balance of materials carried by major world rivers. Mar Chem. 7:173-206. http://dx.doi.org/10.1016/0304-4203(79)90039-2

Mensi Gh S, Moukha S, Creppy EE, Maaroufi K (2008). Metals accumulation in Marine Bivalves and Seawater from theLagoon of Boughrara in Tunisia (North Africa). Int. J. Environ. Res. 2(3):279-284.

Mmolawa K, Likuku A, Gaboutloeloe G (2011). Assess-ment of heavy metal pollution in soils along roadside areas in Botswana. Afr. J. Environ. Sci. Technol. 5(3):186-196.

Mohiuddin KM, Zakir HM, Otomo K, Sharmin S, Shikazono N, (2010). Geochemical distribution of trace metal pollutants in water and sediments of downstream of an urban river. Int. J. Environ. Sci. Tech. 7(1):17-28 http://dx.doi.org/10.1007/BF03326113

Muller G (1969). Index of geoaccumulation in sediments of the Rhine River. J. Geol. 2:108-118.

Muller G (1981). The heavy metal pollution of the sediments of Neckars

and Its Tributary, A Stock taking Chemische Zeit. 150:157-164.
Mumba PP, Chibambo BQ, Kadewa W (2008). A comparison of the levels of heavy metals in cabbages irrigated with reservoir and tap water. Int. J. Environ. Res. 2(1):61-64.
Nabi Bidhendi GR, Karbassi AR, Nasrabadi T, Hoveidi H (2007). Influence of copper mine on surface water quality. Int. J. Environ. Sci. Tech. 4(1):85-91. http://dx.doi.org/10.1007/BF03325965
Nouri J, Mahvi AH, Bazrafshan E (2010). Application of electrocoagulation process in removal of zinc and copper from aqueous solutions by aluminum electrodes. Int. J. Environ. Res. 4(2):201-208.
Nriagu JO (1988). Production and uses of chromium, in: Nriagu JO, Niebner E (Eds.), Chromium in the natural and human environments, Wiley, New York, pp. 81-104.
Okafor EC, Opuene K (2007). Preliminary assessment of trace metals and polycyclic aromatic hydrocarbons in the sediments. Int. J. Environ. Sci. Tech. 4(2):233–240 http://dx.doi.org/10.1007/BF03326279
Priju CP, Narayana AC (2007). Heavy and Trace Metals in Vembanad Lake Sediments. Int. J. Environ. Res. 1(4):280-289.
Ramasamy V, Murugesan S, Mullainathan S (2004). Characterization of minerals and relative distribution of quartz in Cauvery river sediments from Tamilnadu, India- A FTIR study. Bull. Pure Appl. Sci. 23(1-2):1.
Ramasamy V, Murugesan S, Mullainathan S (2005). Distribution and characterization of minerals in Cauvery river sediments by grain size analysis –A new approach by FTIR study. Ind. Miner. 39(2):91-93.
Ramasamy V, Rajkumar P, Ponnusamy V (2006). FTIR spectroscopic analysis and mineralogical characterization of Vellar river sediments. Bull. Pure Appl. Sci. 25(1):49-55.
Ramesh R, Subramanian V, Van Grieken R (1990). Heavy metal distribution in sediments of Krishna river basin, India. Environ Geol. Water Sci. 15:303-324. http://dx.doi.org/10.1007/BF01706412
Saikia BJ, Parthasarathy G, Sarmah NC (2008). Fourier transform infrared spectroscopic estimation of crystallinity in SiO_2 based rocks. Bull. Mater. Sci. 31(5):775-779. http://dx.doi.org/10.1007/s12034-008-0123-0
Sarin MM, Krishnaswami S, Dilli K, Somayajulu BLK, Moore WS (1989). Major ion chemistry of the Ganga–Brahmaputra river system: Weathering processes and fluxes to the Bay of Bengal. Geochim. Cosmochim. Acta. 53:997-1009. http://dx.doi.org/10.1016/0016-7037(89)90205-6
Seralathan P (1987). Trace element geochemistry of modern deltaic sediments of the Cauvery river, east coast of India. Ind. J. Mar. Sci. 16:235-239.
Singh AK (1999). Elemental composition of the Damodar river sediments – A tributary of the Lower Ganga, India. J. Geol. Soc. India 53:219-231.
Singh M, Ansari AA, Muller G, Singh IB (1997). Heavy metals in freshly deposited sediments of the Gomti river (a tributary of the Ganga river): effects of human activities. Environ. Geol. 29:246-252. http://dx.doi.org/10.1007/s002540050123
Singh S, Sarin MM, France-Lanord C (2005). Chemical erosion in the eastern Himalaya: major ion composition of the Brahmaputra and d13C of dissolved inorganic carbon. Geochim. Cosmochim. Acta 69:3573-3588. http://dx.doi.org/10.1016/j.gca.2005.02.033
Singh SK, France-Lanord C (2002). Tracing the distribution of erosion in the Brahmaputra watershed from isotopic compositions of stream sediments. Earth Planet Sci. Lett. 202:645–662. http://dx.doi.org/10.1016/S0012-821X(02)00822-1
Subramanian V (1988). Environmental geochemistry of the Indian river basins: A review. J. Geol. Soc. India. 29:205-220.
Subramanian V, Grieken RV, Dack LV (1987). Heavy metals distribution in the sediments of Ganges and Brahmaputra rivers. Environ. Geol. Water Sci. 9:93-103. http://dx.doi.org/10.1007/BF02449940
Subramanian V, Van't Dack L, Grieken V (1985). Chemical composition of river sediments from the Indian subcontinent. Chem. Geol. 48:271-279. http://dx.doi.org/10.1016/0009-2541(85)90052-X
Tippie V (1984). An environmental characterization of Chesa- peak Bay and a Framework for Action, In: V. Kennedy (Ed.) The Estuary as a Filter, Academic Press, New York. pp. 467-487. http://dx.doi.org/10.1016/B978-0-12-405070-9.50028-1
Tomlinson D, Wilson J, Harris C, Jeffrey D (1980). Pro- blems in the Assessment of Heavy-Metal Levels in Estu-aries and the Formation of a Pollution Index. Helgoland Marine Res. 33(1-4):566-575.
Venugopal T, Giridharan L, Jayaprakash M (2009). Characterization and Risk Assessment Studies of Bed Sediments of River Adyar-An Application of Speciation Study. Int. J. Environ. Res. 3(4):581-598.
Ya ZG, Zhou LF, Bao ZY, Gao P, Sun XW (2007). High efficiency of heavy metal removal in mine water by limestone, Chin. J. Geochem. 28(3):293-298. doi:10.1007/s11631-009-0293-5. http://dx.doi.org/10.1007/s11631-009-0293-5

International Journal of Physical Sciences

academicJournals